

Review

Open Access



Advanced catalysis for efficient hydrogen production

Baoying Dai[#], Chuyi Zhou[#], Hang Yin, Rui Kong, Hao Wang, Yannan Xie

State Key Laboratory of Flexible Electronics (LoFE) and Institute of Advanced Materials (IAM), Jiangsu Key Laboratory for Biosensors, Jiangsu National Synergetic Innovation Center for Advanced Materials (SICAM), Nanjing University of Posts and Telecommunications, Nanjing 210023, Jiangsu, China.

[#]Authors contributed equally.

Correspondence to: Baoying Dai and Prof. Yannan Xie, State Key Laboratory of Flexible Electronics (LoFE) and Institute of Advanced Materials (IAM), Jiangsu Key Laboratory for Biosensors, Jiangsu National Synergetic Innovation Center for Advanced Materials (SICAM), Nanjing University of Posts and Telecommunications, No. 9 Wenyuan Road, Nanjing 210023, Jiangsu, China. E-mail: iambydai@njupt.edu.cn; iamynxie@njupt.edu.cn

How to cite this article: Dai, B.; Zhou, C.; Yin, H.; Kong, R.; Wang, H.; Xie, Y. Advanced catalysis for efficient hydrogen production. *Microstructures* 2025, 5, 2025083. <https://dx.doi.org/10.20517/microstructures.2025.02>

Received: 10 Jan 2025 **First Decision:** 12 Feb 2025 **Revised:** 25 Feb 2025 **Accepted:** 4 Mar 2025 **Published:** 8 Jul 2025

Academic Editor: Zhanxi Fan **Copy Editor:** Ping Zhang **Production Editor:** Ping Zhang

Abstract

Hydrogen energy, characterized by its cleanliness, high energy density, and zero carbon dioxide emissions, is increasingly recognized as a promising alternative to traditional fossil fuels. From this perspective, the highly efficient generation of hydrogen is of paramount importance for mitigating the urgent global energy shortage and environmental challenges. In contrast to conventional fossil fuel-based hydrogen production methods, advanced catalytic technologies that generate hydrogen from water or other renewable resources offer environmentally friendly and sustainable alternatives. In this context, this review exclusively examines the fundamental principles of representative catalytic hydrogen production technologies, encompassing electrocatalytic, piezocatalytic, pyrocatalytic, photocatalytic, and their synergistic catalytic methods at first. Secondly, the latest advancements in the above-mentioned catalytic hydrogen evolution pathways are scrutinized from the perspectives of material composition, structure designs, and hydrogen generation yields. Finally, a comprehensive summary and future outlook for the advancement and practical applications of catalytic hydrogen production technologies are provided. This in-depth review aims to offer both theoretical insights and experimental guidance to researchers in the fields of catalysis, environmental science, energy research, and related areas.

Keywords: Hydrogen production, synergistic catalysis, energy conversion, clean energy



© The Author(s) 2025. **Open Access** This article is licensed under a Creative Commons Attribution 4.0 International License (<https://creativecommons.org/licenses/by/4.0/>), which permits unrestricted use, sharing, adaptation, distribution and reproduction in any medium or format, for any purpose, even commercially, as long as you give appropriate credit to the original author(s) and the source, provide a link to the Creative Commons license, and indicate if changes were made.



INTRODUCTION

The deterioration of the environment and the depletion of fossil fuels have underscored the urgent need for developing renewable and clean sources^[1]. Hydrogen energy, owing to its versatile and efficient attributes, high energy density characteristic, as well as clean and low-carbon nature, is regarded as a rising star in future energy^[2,3]. At present, the production of hydrogen primarily relies on the decomposition of conventional fossil fuels, a process that results in the emission of significant amounts of carbon dioxide, thereby posing a substantial environmental challenge. In this context, advanced catalytic technologies for hydrogen production that are independent of fossil fuels have emerged, encompassing electrocatalytic, piezocatalytic, pyrocatalytic, photocatalytic, and their synergistic catalytic hydrogen production methods, and significant progress have been observed in recent decades^[4]. For example, electrocatalytic hydrogen production technology lies in the conversion of electrical energy into chemical energy through electrocatalysts on the electrodes, achieving the rapid decomposition of water to produce hydrogen and oxygen^[5]. Piezocatalytic hydrogen production is a process that harnesses the built-in electric field generated by piezoelectric materials under mechanical stress to facilitate the water splitting reaction, thereby producing hydrogen in the absence of external power sources^[6]. Pyrocatalytic hydrogen production is realized in the condition of temperature fluctuations in which pyroelectric materials generate pyroelectric polarization charges and consequently catalyze the decomposition of water to yield hydrogen^[7]. Hydrogen production via photocatalytic technology is accomplished using semiconductor photocatalysts that can generate electron-hole pairs upon light irradiation. These pairs subsequently engage in redox reactions with water, thereby facilitating the generation of hydrogen^[8]. Moreover, plenty of catalytic materials with subtle structure and composition designs have been developed, and fascinating synergistic catalytic hydrogen production strategies have emerged in recent years. Therefore, it is imperative to systematically scrutinize the research progress in this field.

Through an extensive review of the literature, we have identified that existing studies predominantly focus on the advancements within a single specific technology, photocatalytic, electrocatalytic, piezoelectric, pyroelectric, or photoelectrocatalytic technology. In these reviews, hydrogen production frequently emerges as a key application area for the specific technology. For example, Teng *et al.* elaborated various coupling methods for photocatalytic hydrogen production, whereas the coupling among photocatalysis with other catalytic methods was not discussed^[9]. Djellabi *et al.* summarized the advancements in multifunctional XTiO_3 perovskite-type oxides that exhibit photocatalytic and piezoelectric properties and their applications in environmental remediation and energy production^[10]. Zhang *et al.* reviewed the progress and applications of pyroelectric materials in the fields of pyroelectric sensing and hydrogen production^[11]. Although these papers have underscored recent advancements in specialized catalytic materials and their applications across energy, environmental, and related domains, the interconnections among piezocatalytic, photocatalytic, pyrocatalytic, and electrocatalytic hydrogen production processes are not scrutinized. In existing reviews, there is an absence of thorough comparative analyses and comprehensive summaries regarding the aforementioned catalytic technologies for hydrogen production.

Hence, this review aims to provide a systematic overview of recent advancements in the field of catalytic hydrogen production. The fundamental principles of advanced electrocatalytic, piezocatalytic, pyrocatalytic, and photocatalytic hydrogen production, as well as their synergistic effects, have been systematically examined, as shown in Figure 1. The representative catalysts with tailored composition, structure, and morphology designed for highly efficient hydrogen generation are mentioned. Furthermore, this paper provides a comprehensive summary and offers a forward-looking perspective on future directions from the viewpoints of mechanism investigation, material design, and energy conversion efficiency to facilitate the development and application of hydrogen production technologies.

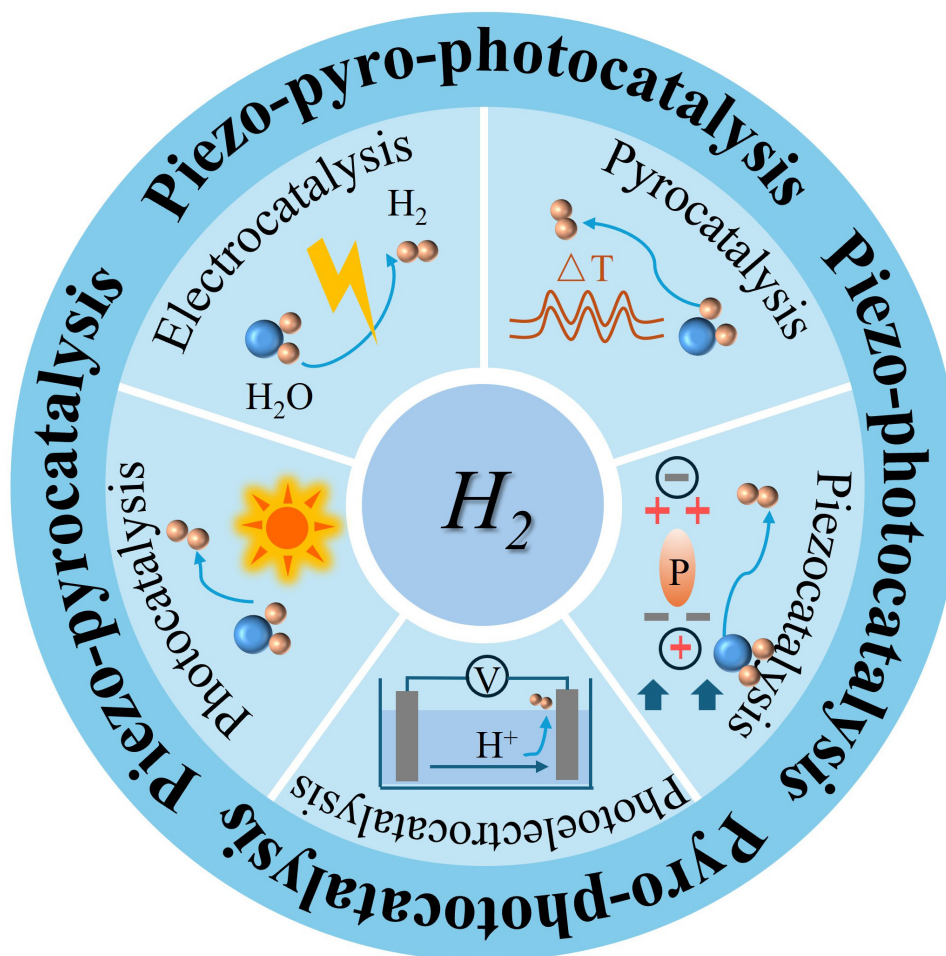


Figure 1. Schematic representation of advanced catalytic technologies for hydrogen production.

ELECTROCATALYTIC HYDROGEN PRODUCTION

Basic principle of electrocatalysis

Electrocatalytic hydrogen production technology mainly involves water electrolysis for hydrogen generation, which lies in the conversion of electrical energy into chemical energy through electrocatalysts on the electrodes, thereby achieving the decomposition of water to produce hydrogen and oxygen. This process includes two half-reactions: the hydrogen evolution reaction (HER) occurring at the cathode and the oxygen evolution reaction (OER) occurring at the anode^[12]. The reaction process of the HER differs in acidic and alkaline electrolytes, yet both conditions entail a two-electron transfer mechanism and a single-step hydrogen atom adsorption-desorption process. In acidic electrolytes, the first step is usually the Volmer reaction, where hydrogen protons are adsorbed onto the catalyst surface and combined with catalytic active sites to yield hydrogen atoms on the catalyst surface. The second step can be divided into the Heyrovsky reaction and the Tafel reaction. The former reaction refers to the process where hydrogen atoms adsorbed on the electrode react with protons or water molecules in the solution to produce hydrogen gas. The latter refers to the process where two hydrogen atoms adsorbed on the electrode combine directly to generate hydrogen gas, which is also known as the coupled desorption step. In the electrocatalytic process, electrons flow from the anode to the cathode through an external circuit, while protons are transported from the anode to the cathode through the electrolyte or proton exchange membrane. The primary chemical reactions occurring during photoelectrocatalytic hydrogen production in acidic conditions can be

described by the following equations:

Cathode (reduction reaction): $4\text{H}_2\text{O} + 4e^- \rightarrow 2\text{H}_2 \uparrow + 4\text{OH}^-$;

Anode (oxidation reaction): $4\text{OH}^- - 4e^- \rightarrow 2\text{H}_2\text{O} + \text{O}_2 \uparrow$;

Total reaction formula: $2\text{H}_2\text{O} \rightarrow 2\text{H}_2 \uparrow + \text{O}_2 \uparrow$.

Under alkaline conditions, the kinetics of HER is generally slower than that under acidic conditions due to the lower concentration of protons in alkaline media. Therefore, the HER process requires the dissociation of water near the catalyst surface to obtain protons, and the reaction pathway of HER may proceed via the Volmer-Tafel mechanism or the Volmer-Heyrovsky mechanism. As a result, the activity and exchange current density of catalysts in alkaline solutions are lower compared to those observed under acidic conditions. The corresponding HER and OER, which involve the transfer of protons (H^+), can be described as follows:

Cathode (reduction reaction): $4\text{H}^+ + 4e^- \rightarrow 2\text{H}_2 \uparrow$;

Anode (oxidation reaction): $2\text{H}_2\text{O} - 4e^- \rightarrow \text{O}_2 \uparrow + 4\text{H}^+$;

Total reaction formula: $2\text{H}_2\text{O} \rightarrow 2\text{H}_2 \uparrow + \text{O}_2 \uparrow$.

Advancements in electrocatalytic hydrogen production

Owing to its high current density, stability, relatively low equipment costs, and ease of operation, electrocatalytic HER has garnered significant attention, and plenty of fascinating electrocatalysts exhibiting high HER performance have been developed, which can be mainly classified into the following five types: precious metal-based, transition metal-based, non-metal-based catalysts, as well as metal-organic frameworks-based and covalent organic frameworks-based catalysts. Some of the typical electrocatalysts for hydrogen production are summarized in Table 1.

Transition metal-based electrocatalysts

Transition metal-based catalysts, possessing advantages such as metallic-like properties, abundant resources, tunable composition, and high cost-effectiveness, have emerged as highly attractive alkaline electrocatalytic materials, including nickel-based materials (e.g., nickel metal, nickel-based alloys, nickel-based composites, and porous nickel), transition metal phosphides (TMPs), and low-dimensional transition metal dichalcogenides (TMDs)^[13]. Compared to nickel-based catalysts, TMPs have multiple active centers and adjustable electronic structures, thus presenting superior HER performance. Bai *et al.* systematically summarized the advancements of TMPs in enhancing HER performance through atomic doping engineering, highlighting the critical role of metallic dopants (such as Ni, Co, Fe, Mn, Mo, Al) and nonmetallic dopants (such as B, S, N, O, F) in modulating the electronic structure, adjusting the d-band center position, and optimizing the hydrogen adsorption Gibbs free energy, thereby significantly improving HER performance^[14]. For example, Kim *et al.* corroborated that the HER activity of TMPs can be improved through atomic doping engineering strategy^[12]. Specifically, by atomic doping V atoms into CeO_2 structure, the electronic structure of CeO_2 was adjusted, Gibbs free energy for hydrogen evolution was lowered, the d-band center was modified, an increase in electron density of 0.01~0.03 was obtained, and the kinetics of HER was strikingly boosted by 1.8 times.

Table 1. Summary of typical catalytic H₂ production methods and corresponding representative catalysts with specific hydrogen evolution efficiencies

Methods	Materials	Experimental conditions	H ₂ production efficiency	Ref.
Electrocatalysis	2D MoSe ₂	0.5 M H ₂ SO ₄ solution	105 mV (vs. RHE) at 10 mA cm ⁻²	[15]
	P-mAuRh	1 M KOH containing 0.33 M urea, loading 0.5 mg cm ⁻²	1.47 V (vs. RHE) at 100 mA cm ⁻²	[17]
	Pt ₇ IrNB	N ₂ -saturated 0.5 M H ₂ SO ₄ solution, a conventional three-electrode	20 mV (vs. RHE) at 10 mA cm ⁻²	[18]
	CoxFe _{1-x} P	1 M KOH solution, a modified glassy carbon rotation disk electrode (5 mm diameter)	294 mV (vs. RHE) at 10 mA cm ⁻²	[21]
Piezocatalysis	Ti ₃ C ₂	0.5 M Na ₂ SO ₄ solution, ultrasonic cleaner (45 kHz, 600 W)	184 μmol g ⁻¹ h ⁻¹	[24]
	UiO-66(Zr)-F ₄	110 W ultrasonic vibration (40 kHz)	178.5 μmol g ⁻¹ h ⁻¹	[25]
	R3c LiNbO ₃ -ZnSnO ₃	150 W Xe lamp, 250 W ultrasonic vibration (40 kHz)	3,453.1 μmol g ⁻¹ h ⁻¹	[22]
Pyrocatalysis	Hexagonal CdS	25-55 °C heating-cooling cycles	4.3 μmol g ⁻¹ cycle ⁻¹	[26]
	PZT sheet	0.5 M KOH electrolyte, 43-46 °C heating-cooling cycles	0.654 μmol h ⁻¹	[27]
Photocatalysis	MC-CN	loaded with Rh and Cr ₂ O ₃ as the cocatalyst, λ > 420 nm	57 μmol g ⁻¹ h ⁻¹	[28]
	1D/2D CoS _{1.097} @ZIS	420 nm and 780 nm cutoff filters, excitation wavelength of 320 nm	2,632.33 μmol g ⁻¹ h ⁻¹	[29]
Photoelectrocatalysis	CuI/TiO ₂	0.1% v/v concentration of triethanolamine, 300 W xenon lamp with an AM 1.5 G filter	9.6 μmol h ⁻¹	[30]
	HOFs@Fe ³⁺	20 min under visible light irradiation	21.55 mmol g ⁻¹ h ⁻¹	[31]
	In ₂ O ₃ /ZnIn ₂ S ₄	H ₂ PtCl ₆ added to produce Pt as co-catalyst, visible light irradiation	2.18 mmol g ⁻¹ h ⁻¹	[32]
Piezo-photocatalysis	Pt/ZnIn ₂ S ₄ /BaTiO ₃	50 mL of 5-Hydroxymethylfurfural aqueous solution (0.1 M), 300 W xenon lamp with a 420 nm cutoff filter, 100 W ultrasonication	1,335.3 μmol g ⁻¹ h ⁻¹	[62]
	SrTiO ₃ /BaTiO ₃ nanofiber	0.5 M Na ₂ SO ₄ solution, 300 W xenon lamp with intensity of 100 mW cm ⁻² , 90 W ultrasonication	1,950.2 μmol g ⁻¹ h ⁻¹	[63]
Pyro-photocatalysis	BaTiO ₃ nanorods	0.1 M Na ₂ SO ₄ and 0.1 M potassium phosphate, 20-50 °C heating-cooling cycles, 300 W xenon lamp with an AM 1.5G filter	13.44 μmol cm ⁻²	[65]
	NaNbO ₃ films	20-50 °C heating-cooling cycles, visible light irradiation	4.57 μmol h ⁻¹	[66]
Piezo-pyro-photocatalysis	PVDF/Fe ₃ O ₄ @g-C ₃ N ₄	magnetic stirring 200 rpm, 20-68 °C heating-cooling cycles, xenon lamp irradiation	42.3 μmol h ⁻¹	[64]

RHE: Reversible hydrogen electrode; PZT: PbZrTiO₃; MC-CN: monomolecular carbohydrazide-carbon nitride; HOFs: hydrogen-bonded organic frameworks; PVDF: polyvinylidene fluoride.

MoSe₂, as a representative low-dimensional TMD, has aroused intensive attention for electrocatalytic hydrogen production. MoSe₂ that exists in a stable 2H phase exhibits semiconductor properties, and the electrocatalytic performance can be observed at its flaky edges, significantly restricting its overall HER performance. To solve this problem, Zhang *et al.* developed a strategy to comprehensively activate TMDs by inserting two-dimensional MoSe₂ and two-dimensional CoP, where the unique interlayer structure increased the active surface area by ten times and the boosted interface enabled rapid ion/electron transport, leading to improved conductivity. As shown in Figure 2A, a notable Tafel slope of 162 mV dec⁻¹ was observed over MoSe₂/CoP hybrid, which was much smaller than pristine MoSe₂ and CoP, suggesting its improved reaction kinetics of HER. Furthermore, the MoSe₂/CoP intercalated hybrids exhibited a remarkably lower charge transfer impedance (6.4 Ω) than those detected over MoSe₂ (34 Ω) and porous CoP nanosheets (17.6 Ω) [Figure 2B], which further endowed MoSe₂/CoP with an increased current intensity of 10 mA cm⁻² and a lowered overpotential of 120 mV [vs. reversible hydrogen electrode (RHE)] [Figure 2C]^[15]. Moreover, Saha *et al.* demonstrated that fully exfoliated 1T phase MoS₂ nanosheets with high water dispersibility can be obtained over TiO₂-single or weakly stacked MoS₂ nanosheets, which not only enhanced the amount of active edge sites but also improved its conductivity. As a result, an overpotential of

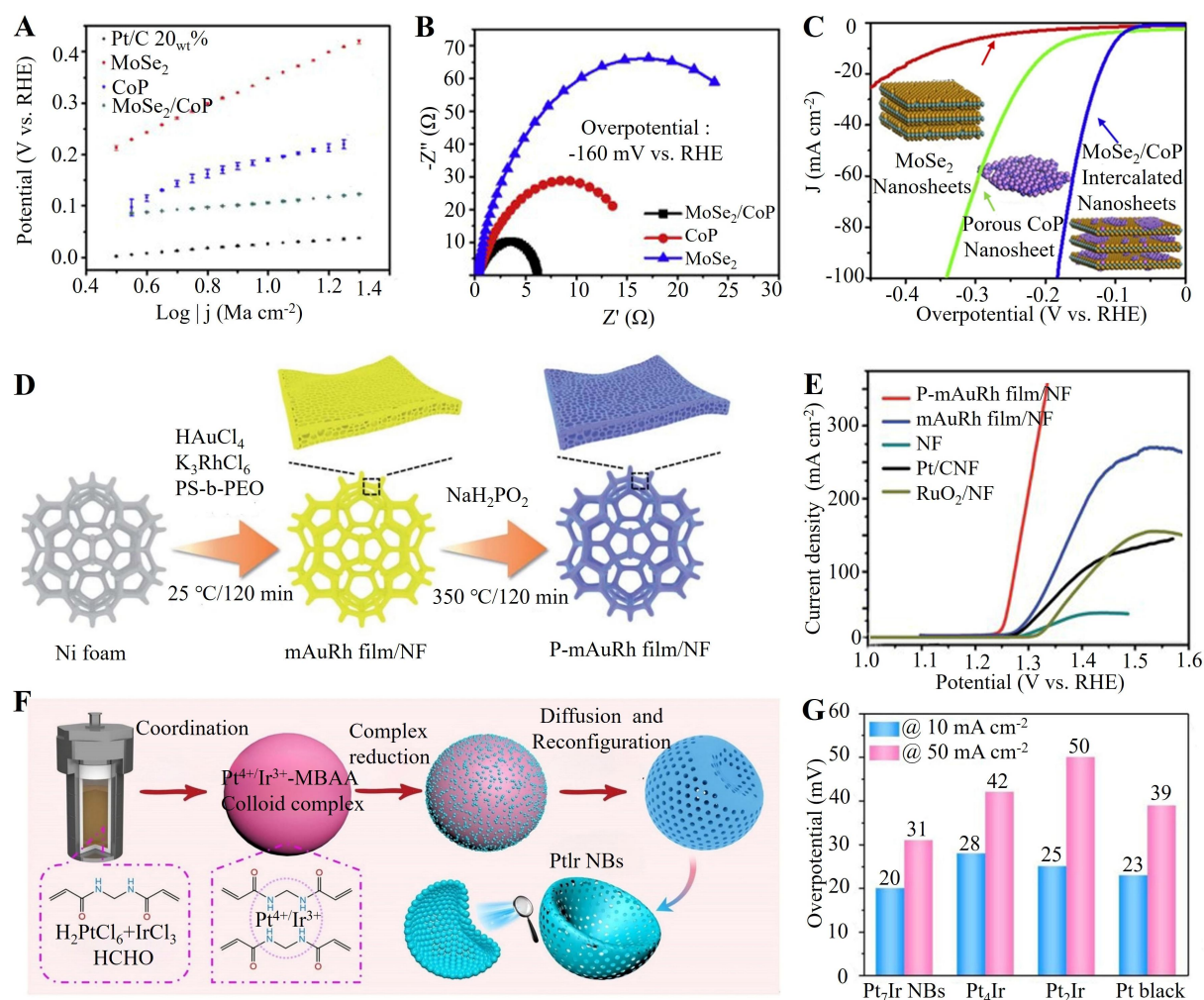


Figure 2. Electrocatalytic hydrogen production. (A) Tafel slope, (B) electrochemical impedance spectra recorded at a biased potential of -160 mV vs. RHE, and (C) overpotentials of MoSe₂, CoP, and exfoliated colloidal MoSe₂/CoP nanosheets. Figure A-C are quoted with permission from Zhang et al.^[15]; (D) Schematic diagram of the fabrication process of the P-mAuRh film/NF, and (E) the corresponding current density of the prepared samples under different potentials. Figure D and E are quoted with permission from Zhang et al.^[17]; (F) Schematic representation of the synthesis mechanism of hollow porous PtIr nanobowls, and (G) the corresponding overpotentials of the prepared samples at different current densities. Figure F and G are quoted with permission from Zhang et al.^[18]. RHE: Reversible hydrogen electrode.

56 mV/decade was observed for HER reaction^[16]. These results suggest that high-efficient electrocatalysts for hydrogen production can be achieved by modulating the material crystal phase and electronic structures.

Non-metal-based electrocatalysts

Non-metal-based catalysts predominately refer to carbon-based electrocatalysts, such as graphene, carbon nanotubes (CNTs), and porous carbon materials. The unique physicochemical properties, e.g., excellent conductivity, a large specific surface area, and good chemical stability, impart these non-metal-based catalysts with great potential in water electrolysis for hydrogen production. For example, Chen *et al.* demonstrated that the defects on reduced graphene oxide (rGO) over CoP/rGO with platinum-like activity can not only serve as nucleation sites for the uniform growth of CoP nanoparticles, but also generate more isolated electrons, altering the local charge state around the defects, optimizing the Gibbs free energy absorption and thus improving HER activity^[1]. This defect-engineered rGO offered a viable alternative to

precious metals for electrocatalytic hydrogen production. In addition, Zhang *et al.* reported a self-supported P-mAuRh film/NF membrane [Figure 2D], which functions as both an anode and cathode catalyst, demonstrating the capability to effectively drive urea-assisted overall water electrolysis^[17]. As Figure 2E shows, the constructed P-mAuRh film/NF sample exhibited much higher current density under the same potential than those detected over mAuRh film/NF, NF, Pt/CNF, and RuO₂/NF, highlighting the great hydrogen evolution capability of P-mAuRh film/NF. The enhanced electrocatalytic overall water splitting performance was attributed to the synergistic effect of the mesoporous film nanostructure, the optimized bimetallic composition, and the electronic interactions between metals and non-metals. The previous studies indicated that non-metal-based electrocatalysts play a crucial role in facilitating both OER and HER catalysis.

Precious metal-based electrocatalysts

Precious metal-based electrocatalysts primarily consist of Pt, Ir, Pd, Ru, and Rh. Among these, platinum exhibits significantly superior HER performance, attributed to the free energy of hydrogen adsorption intermediates on Pt being closest to the ideal value of zero. In response to the growing demand for environmental protection and renewable energy, the development of electrocatalysts for hydrogen production with superior activity and stability has garnered considerable attention. Recently, Zhang developed a self-template strategy to synthesize hollow and porous bowl-shaped Pt-Ir alloy nanocrystals, which are composed of ultra-ruthenium nanoparticles with an average size of 2.4 nanometers [Figure 2F]^[18]. These nanocrystals have a high surface atom ratio and abundant active sites, which can reduce the consumption of expensive precious metals and provide sufficient molecular permeability. The tunable electronic structures, 3D availability of both inner and outer surfaces, and high atomic utilization efficiency of this bimetallic alloy catalyst further endowed it with a much lower overpotential of 20 and 31 mV at 10 and 50 mA cm⁻², respectively [Figure 2G]. Additionally, Kim *et al.* proposed that Re, which exhibits electrocatalytic activity similar to Pt but is more cost-effective, was a promising alternative to precious Pt catalysts^[12]. To validate this hypothesis, they synthesized clusters of Re nanoparticles doped with trace amounts of platinum and nickel (Pt-Ni@Re/C), which were interconnected by an amorphous carbon matrix, showcasing an obviously enhanced hydrogen desorption energy of 0.34 eV over Pt-Ni@Re (0001). These investigations imply that the development of precious metal alloys and other cost-effective alternatives is both feasible and essential for advancing the establishment of industrial green hydrogen production systems.

Metal-organic frameworks and covalent organic frameworks

In addition to the aforementioned electrocatalysts, materials developed based on metal-organic frameworks (MOFs) and covalent organic frameworks (COFs) represent two emerging and promising branches in electrocatalytic hydrogen production, attributed to their high specific surface area, tunable porosity, and structural diversity^[19]. These composite materials not only preserve the inherent advantages of carbon-based materials but also exhibit characteristics unique to non-carbon materials, thereby significantly enhancing electrocatalytic hydrogen generation performance. Moreover, it is reported that various strategies can be employed to improve the catalytic performance of the original MOFs, such as increasing the conductivity of MOFs by constructing with conductive particles or substrates, reducing the thickness of MOF nanosheets, introducing structure defects, and so on^[20]. For instance, Zhang *et al.* synthesized a subtle MOF electrocatalyst Co₃Fe_{1-x} with metallic-like properties due to the presence of phosphorus in the compound, which significantly improved the conductivity of the prepared MOF catalyst. As a consequence, a decreased overpotential of 1.51 V (*vs.* RHE from 10⁵ to 0.01 Hz with 5 mV) was required for HER^[21]. These findings highlight that the designability of structures within MOFs and COFs offers a promising avenue to enhance the HER performance of these two classes of electrocatalytic materials, and it is essential to optimize the

defects, surface and conjugate ligands, metal nodes, and functional linkers of MOFs and COFs for realizing high-efficient HER.

Although electrocatalytic hydrogen production is emerging as a promising energy carrier with numerous advantages, it still faces significant challenges compared to traditional fossil fuels. The primary hurdles revolve around the dual constraints of energy conversion efficiency and economic viability. Most currently employed electrocatalysts rely heavily on precious metals such as platinum and iridium, which substantially increase costs and hinder the large-scale deployment of this technology. Additionally, the degradation of catalytic active sites under prolonged exposure to high potentials and highly corrosive environments remains unresolved, impacting the overall system longevity. Addressing these issues necessitates a focus on optimizing material synthesis for large-scale production while ensuring the uniformity and stability of catalysts. At first, a multiscale collaborative design approach is essential, emphasizing material structure regulation, precise synthesis processes, and scalability for mass production. Catalyst design should prioritize the development of robust active site anchoring mechanisms, leveraging strong interactions or confinement effects between the support and active components to mitigate particle migration and agglomeration. Concurrently, interface engineering can be employed to optimize electronic structures, thereby enhancing intrinsic catalytic activity. During synthesis, dynamic control over nucleation, growth, and loading stages must be rigorously enforced, guided by theoretical simulations to fine-tune process parameters and ensure the uniform distribution of active sites. For large-scale production, the development of continuous and modular synthesis routes is critical. This can be achieved through innovative reactor design and process optimization to ensure batch consistency. Enhancing stability requires a dual focus on chemical stability and mechanical durability. Incorporating self-healing functionalities or anti-corrosion interface layers can help mitigate the effects of extreme potentials and corrosive media during electrolysis. Additionally, establishing accelerated aging testing systems will enable the quantification of lifespan decay patterns, providing insights for further improvements. Ultimately, a cross-scale collaborative innovation strategy, spanning materials, processes, and equipment, can achieve comprehensive optimization from atomic-level activity regulation to macro-engineering manufacturing. This holistic approach will balance the cost-effectiveness of large-scale production with the long-term reliability of catalytic systems, paving the way for the widespread adoption of electrocatalytic hydrogen production.

PIEZOCATALYTIC HYDROGEN PRODUCTION

Basic fundamentals of piezocatalytic hydrogen production

There are two basic theories describing the piezocatalytic hydrogen production process: charge screening effect and energy band theory. The former theory attributes the role of the excited electrons and holes of piezoelectric materials under the applied mechanical force, and these electrons and holes then take part in redox reactions with water and oxygen to generate hydrogen [Figure 3A]. The later theory highlights piezocatalytic hydrogen evolution to the screening charges absorbed on the surface of piezoelectric materials, which participate in redox reactions with oxygen and water, giving access to the formation of hydrogen [Figure 3B]. In the above process, the piezoelectric field formed on the surface of piezoelectric material will lead to energy band bending, thereby promoting electrons and holes migration, facilitating hydrogen evolution efficiency. In both theories, the piezocatalytic hydrogen production rates are predominantly dependent on the piezoelectric potential output, which is related to the piezoelectric property of piezocatalytic material and the applied mechanical force.

Progress in piezocatalytic hydrogen generation

Compared with electrocatalytic technology, piezocatalytic hydrogen production technology offers a novel approach to generating green hydrogen by harnessing environmental mechanical energy sources, eliminating the need for additional electrical energy input. It makes the direct conversion from mechanical

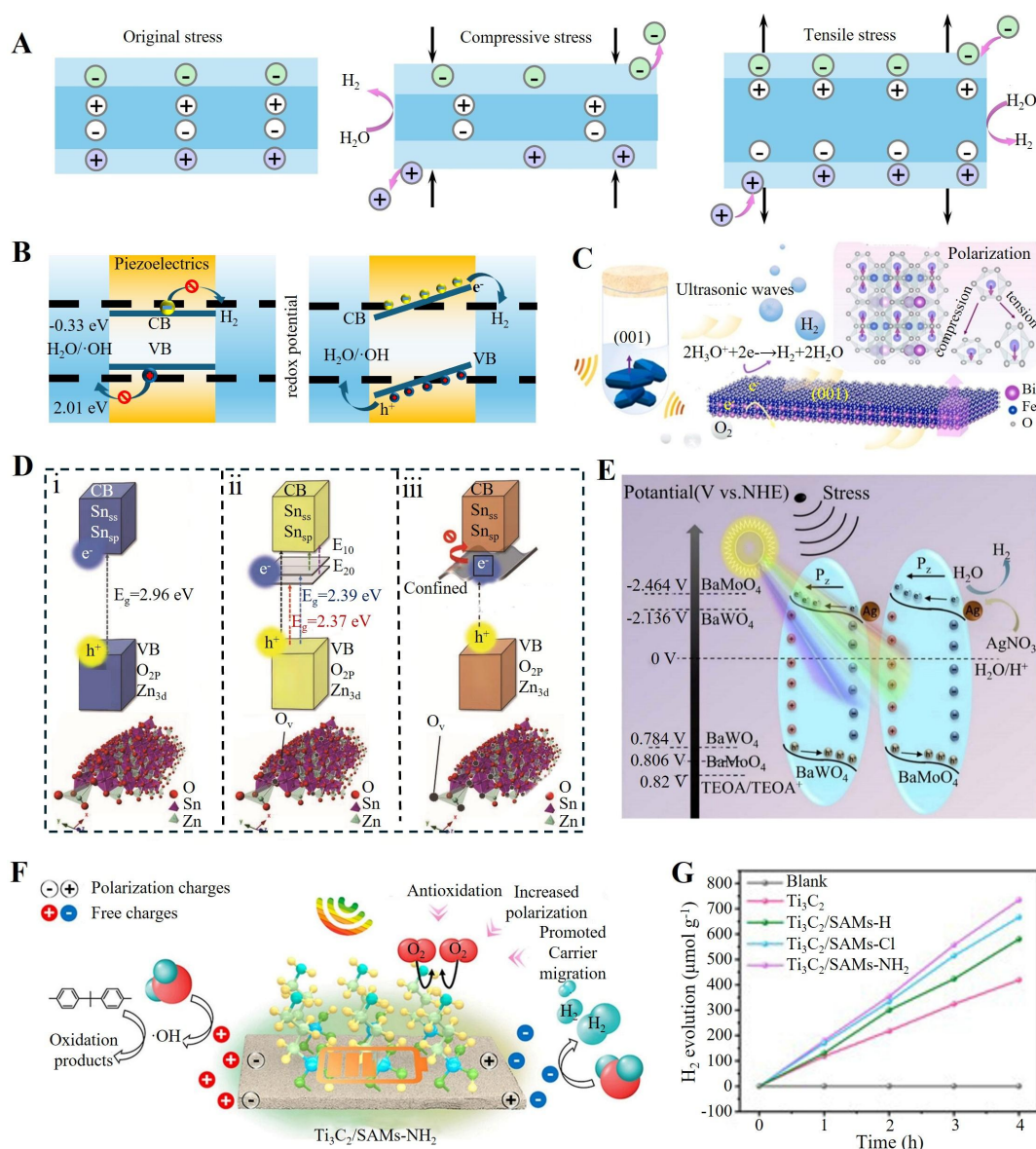


Figure 3. Schematic diagrams illustrating piezocatalytic hydrogen production process based on (A) charge screening effect and (B) energy band theory; (C) Schematic diagram of piezocatalytic hydrogen production process over $Bi_2Fe_2O_9$ nanosheets. This figure is quoted with permission from Du et al. [6]; (D) Schematic diagram presenting the crystal structures of (i) pristine $ZnSnO_3$ and $ZnSnO_3$ NWs with (ii) moderated and (iii) excessive oxygen vacancies for hydrogen production. This figure is quoted with permission from Wang et al. [22]; (E) Schematic illustration of the piezocatalytic hydrogen production process of $BaMoO_4$ - $BaWO_4$ -Ag. This figure is quoted with permission from Kuru et al. [23]; (F) Schematic diagram illustrating the mechanism of piezocatalytic degradation of bisphenol A (BPA) and hydrogen production by $Ti_3C_2/SAMs-NH_2$, and (G) the corresponding H_2 production rates. Figure F and G are quoted with permission from Wang et al. [24].

energy into chemical energy possible, and thus has sparked significant research interest. In recent years, significant advancements have been made in the fundamental investigations of piezocatalytic processes, piezocatalytic material modifications to achieve partial and overall water splitting, and the development of strategies for performance enhancement. Some typical piezocatalysts with fascinating hydrogen generation performance are summarized in Table 1.

It is widely reported that piezoelectric materials can be defined into three types - inorganic piezoelectric, organic piezoelectric, and organic-inorganic piezoelectric composites. At current stage, piezoelectric materials reported for hydrogen production are focused on inorganic piezocatalytic materials attributed to their higher electromechanical coupling coefficient. For instance, Du *et al.* investigated the piezocatalytic hydrogen production performance of $\text{Bi}_2\text{Fe}_4\text{O}_9$, and found that $\text{Bi}_2\text{Fe}_4\text{O}_9$ nanosheets with a centrosymmetric structure demonstrated exceptional piezoelectric catalytic performance in the degradation of hydrogen-evolving organic compounds [Figure 3C]^[6]. To further improve the piezocatalytic hydrogen evolution rate, some modification strategies have been proposed, e.g., morphology control, strain engineering, heterostructure construction, defect engineering, metal loading, and so on. For example, Wang *et al.* synthesized R3c-ZnSnO_3 with different oxygen vacancy densities and explored the impact of oxygen vacancy within crystal structure and the consequently varied spontaneous polarization on piezocatalytic hydrogen production efficiency. The results indicated that the controlled oxygen vacancies within the crystal lattice not only functioned as donor sites to facilitate the excitation of free carriers to the conduction band (CB), thereby enhancing their participation in the reduction reaction to produce hydrogen, but also acted as a donor band to prolong the electron lifetime [Figure 3D]^[22]. As a consequence, an obvious hydrogen production rate of $3,453.1 \mu\text{mol g}^{-1} \text{h}^{-1}$ was observed. In addition, Kuru *et al.* constructed scheelite-type BaWO_4 and BaMoO_4 into heterojunction, with *in-situ* piezoelectric deposited Ag on its surface, to achieve efficient piezoelectric hydrogen production [Figure 3E]^[23]. The result suggested that the Schottky junction formed between the interface of BaWO_4 - BaMoO_4 and Ag facilitated the separation and migration of electrons and holes, leading to a higher piezocatalytic hydrogen evolution rate of $313 \text{ mmol g}^{-1} \text{h}^{-1}$.

Although inorganic piezoelectric materials exhibit potential in hydrogen evolution, traditional inorganic piezoelectric materials frequently encounter limitations, including a wide bandgap and inadequate charge carrier transport, which impede the enhancement of their hydrogen evolution efficiency. In this context, polar materials with spontaneous polarization (Ps) have aroused intensive attention for realizing piezocatalytic hydrogen evolution. For example, Wang *et al.* constructed a polar self-assembled monolayers- NH_2 (SAMs- NH_2) on the surface of Ti_3C_2 to enhance its environmental stability and piezocatalytic activity^[24]. The surface-treated Ti_3C_2 exhibited different lattice parameters and symmetries, and the presence of polar functional groups SAMs- NH_2 further increased the surface potential of Ti_3C_2 , facilitating the migration of piezoelectrons [Figure 3F]. As a result, the highest hydrogen production efficiency of $184 \mu\text{mol g}^{-1} \text{h}^{-1}$ over Ti_3C_2 /SAMs- NH_2 was achieved under ultrasonic vibration [Figure 3G]. Furthermore, Shi *et al.*^[25] designed a novel UIO-66(Zr)-F4 MOF nanosheet for piezocatalytic water splitting, which presented a hydrogen generation rate of $178.5 \mu\text{mol g}^{-1}$ under ultrasonic vibration excitation (110 W, 40 kHz) for 5 h. Their work highlighted the potential of MOF-based porous piezocatalytic nanomaterials in harnessing mechanical energy to drive chemical reactions. These works indicate that material morphology and structure design play a crucial role in determining piezocatalytic hydrogen production performance, and it is important to craft piezocatalysts for achieving high-efficient hydrogen generation.

Although piezoelectric systems hold immense potential for capturing environmental mechanical energy and converting it into hydrogen energy, significant challenges must be overcome to transition from laboratory research to real-world applications. For instance, the current energy conversion efficiency under mechanical field conditions is less than 5%, far below the theoretical maximum efficiency of over 30%. This gap severely limits the practical application of piezocatalytic technology for hydrogen evolution. Additionally, persistent issues such as fatigue degradation under prolonged cyclic mechanical loads and scalability constraints in hybrid energy harvesting architectures remain unresolved. Addressing these challenges requires the development of piezocatalysts that exhibit long-term stability, cost-effectiveness, and high energy

conversion efficiency. Furthermore, the stability of hydrogen evolution in piezocatalytic technology is significantly influenced by mechanical forces, such as ultrasonication and ocean waves. Ultrasonication requires external energy input, while ocean waves exhibit inherent variability, leading to an unstable hydrogen generation process compared to the hydrogen production pathways based on fossil fuels. Therefore, it is imperative to foster collaboration in infrastructure sharing and supply chain optimization to support large-scale hydrogen production initiatives. These strategies are essential for advancing the practical deployment of piezoelectric energy harvesting technologies and unlocking their full potential.

PYROCATALYTIC HYDROGEN PRODUCTION

Basic principle of pyrocatalytic hydrogen generation

The basic principle of pyrocatalytic hydrogen evolution refers to the process that pyroelectric materials generate positive and negative polarization charges under environmental temperature fluctuations, and the absorbed screening charged take part in redox reactions with water and oxygen to form hydrogen [Figure 4A]. This process is similar to piezocatalysis, except that the stimulus is changed from the applied force to the environmental temperature fluctuations. Furthermore, the pyrocatalytic hydrogen production efficiency greatly relies on the generation of pyroelectric polarization charges of pyroelectric materials, depending on the pyroelectric property of pyroelectrics and temperature heating and cooling rates.

Advancements in pyrocatalytic hydrogen production

Although pyrocatalytic hydrogen production presents a routine to directly convert temperature into chemical energy and temperature fluctuations are ubiquitous in the environment, the temperature heating or cooling rates are too small to effectively drive pyrocatalytic hydrogen production. At present, the temperature fluctuations employed for driving pyrocatalysis are regulated through controlled heating and cooling systems, severely hindering the practical applications of pyrocatalytic technology in hydrogen production. In this context, significant efforts have been devoted to the design and optimization of the composition, crystal phase, and morphology of pyrocatalytic materials, and plenty of pyrocatalytic materials have been developed for hydrogen production. Some representatives are listed in Table 1.

To realize high-efficient pyrocatalytic hydrogen production, Zhang *et al.* employed organic molecule 2-mercaptobenzimidazole (2MBI) to modify the surface of CdS nanorods, a widely studied zinc-blende structured semiconductor with a pronounced pyroelectric effect [Figure 4B]. The results indicated that 2MBI with excellent bonding characteristics and strong hole acceptor ability was beneficial for enhancing the pyroelectric responses of CdS to temperature fluctuations, boosting the separation of pyroelectric-induced charges, and ultimately leading to a higher pyrocatalytic hydrogen evolution activity of 5 folds of that for CdS alone [Figure 4C]^[26]. This work demonstrates the important role of surface modification in facilitating pyrocatalytic hydrogen evolution efficiency. In addition, Zhang *et al.* proposed an innovative approach for pyrocatalytic hydrogen generation utilizing low-grade waste heat or ambient temperature fluctuations through the thermal cycling of water decomposition, and the designed equipment was depicted in [Figure 4D]^[27]. They systematically investigated the impact of electrolyte concentration and heating-cooling frequency on pyrocatalytic hydrogen production performance, and the results indicated that the pyrocatalytic material PbTiO₃ (PZT) sheet tailored with nanostructures exhibited a higher hydrogen evolution rate of 3.93 μmol in 6 h due to the increased surface area. More significantly, this work provides an available and sustainable paradigm for realizing pyrocatalytic hydrogen production by utilizing waste temperature.

Furthermore, You *et al.* introduced a localized plasmonic heat source to rapidly and efficiently heat the coke pyrocatalytic material itself by *in-situ* growing Au nanoparticles on three-dimensional coral-like BaTiO₃,

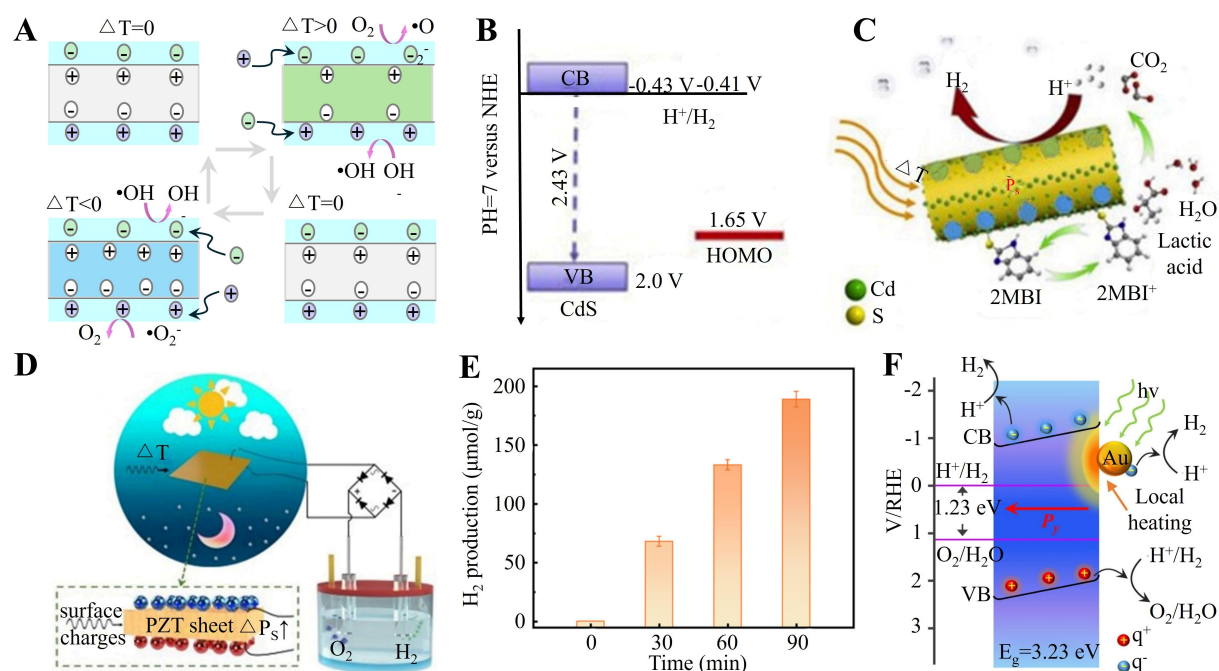


Figure 4. Pyrocatalytic hydrogen production. (A) Schematic diagram showing the basic principle of pyrocatalytic hydrogen evolution; (B) The energy levels of CdS nanorod catalysts and the HOMO energy level of 2MBI, and (C) pyrocatalytic hydrogen production pathway over the prepared CdS-2MBI sample under cold-hot alternation excitation. Figure B and C are quoted with permission from Zhang et al.^[26]; (D) Schematic diagram of PZT sheet generating pyroelectricity and splitting water into hydrogen. This figure is quoted with permission from Zhang et al.^[27]; (E) Schematic illustration of pyrocatalytic hydrogen generation of Au/BaTiO₃ nanoparticles driven by surface plasmon local heating, and (F) the corresponding normalized H_2 production rates (normalized to the production rate of Au/BaTiO₃ NPs) of different samples under the irradiation by a 532 nm nanosecond laser. Figure E and F are quoted with permission from You et al.^[28]. HOMO: Highest occupied molecular orbital; PZT: PbZrTiO₃.

nanoparticles^[28]. The constructed plasmonic metal/coking pyrocatalytic composite material showcased a rapid temperature heating rate of 100 K within a distance of around 1 μm of an Au nanoparticle (around 40 nm) under pulsed laser (wavelength centering at 532 nm) irradiation, giving access to a high hydrogen evolution activity of about $133 \mu\text{mol g}^{-1} \text{h}^{-1}$ [Figure 4E]. They contributed the notable pyrocatalytic hydrogen evolution performance to the localized surface plasmon resonance (LSPR) effect of Au nanoparticles, as illustrated in Figure 4F. Under light illumination, the LSPR effect of Au nanoparticles resulted in localized heating of the BaTiO₃ nanoparticles. The resultant uncompensated pyroelectric charges on the BaTiO₃ nanoparticles participated in the reduction reaction with surrounding water molecules to generate hydrogen. Upon cessation of light irradiation, the temperature of the BaTiO₃ nanoparticles decreased due to thermal dissipation into the surrounding water. In this cooling process, the uncompensated pyroelectric surface charges once again facilitated the pyrocatalytic water splitting reaction. Notably, the built-in electric field originating from surface pyroelectric charges played a positive role in facilitating charge separation and transfer during the aforementioned heating-cooling cycle, leading to efficient pyrocatalytic hydrogen production. These studies have demonstrated that the pyrocatalytic hydrogen production efficiency of pyrocatalysts can be significantly enhanced through surface modification and multifunctional design. Although environmental waste heat has been harnessed for pyrocatalytic hydrogen production, the current hydrogen evolution efficiency remains low.

The core challenge currently facing pyroelectric catalytic hydrogen production technology lies in the multi-field coupling efficiency of thermal, electrical, and chemical energy, as well as the compatibility of the material system. The pyroelectric effect relies on the polarization charges generated by materials during

temperature changes to drive catalytic reactions. However, the pyroelectric coefficients of materials are generally low, and they are prone to lattice distortion or phase changes during thermal cycling, leading to a reduction in polarization strength. At the same time, the efficiency of charge carrier generation and separation induced by temperature gradients is insufficient, resulting in a significant amount of charge recombining in bulk or at interfaces, which reduces the effective utilization of catalytic active sites. Furthermore, the stability of the catalyst interface in a thermally fluctuating environment is poor, and repeated thermal stress can easily cause material cracking or the peeling of the active layer, exacerbating performance degradation. To effectively overcome these bottlenecks, a comprehensive and synergistic approach is required, focusing on both material optimization and system design innovation. This entails: (1) developing advanced ferroelectric materials with enhanced thermal stability and broad temperature response ranges through strategic doping and defect engineering to optimize their band structures and charge carrier migration pathways; (2) engineering heterojunctions and gradient interfaces to facilitate efficient directional separation and rapid transport of thermally generated charges; (3) incorporating adaptive buffer layers and flexible substrates to alleviate mechanical degradation caused by thermal stress in catalytic structures; and (4) implementing *in-situ* characterization techniques to enable real-time monitoring of interface evolution during thermal-electrical-chemical coupling processes, thereby informing stability-enhancing design strategies. Furthermore, the development of advanced thermal management systems for efficient utilization of temperature fluctuations will significantly reduce dependence on continuous external heating, contributing to overall system optimization.

PHOTOCATALYTIC HYDROGEN PRODUCTION

Basic principle of photocatalytic hydrogen evolution

Photocatalytic principle is developed based on semiconductors. During the photocatalytic hydrogen evolution process, as depicted in [Figure 5A](#), the semiconductor is irradiated by the photons with energy higher or equal to the energy bandgap of semiconductor photocatalysts, and electrons are excited from the valence band (VB) to the CB, generating the same number of holes on the VB. Some of these electrons and holes separate and then migrate to the surface, where the absorbed water undergoes reduction with electrons, producing hydrogen. The other part of electrons and holes get recombined inside or on the surface of photocatalyst, restricting photocatalytic hydrogen production efficiency. It can be inferred that the photocatalytic hydrogen production rate is predominately determined by the light absorption rate, carrier separation and transfer rate, and surface reduction reaction rate.

Progress in photocatalytic hydrogen production

Based on the photocatalytic hydrogen production process, plenty of strategies have been proposed for improving hydrogen generation efficiency, focusing on increasing light absorption efficiency, suppressing photoexcited carrier recombination, and accelerating surface reaction kinetics. A variety of photocatalysts have been developed to split water into hydrogen, and some typical representatives are summarized in [Table 1](#). These photocatalysts can be classified into three categories based on their energy bandgap characteristics: ultraviolet-light-responsive photocatalysts with wide bandgaps, visible-light-responsive photocatalysts featuring medium bandgaps or heterojunction structures, and infrared-light-responsive photocatalysts characterized by narrow bandgaps or hybrid compositions.

Ultraviolet-light-responsive photocatalysts

Photocatalysts that respond to ultraviolet (UV) light are predominantly composed of wide bandgap semiconductor materials, such as TiO_2 and ZnO . Despite UV light having higher energy compared to visible and infrared light, it constitutes less than 5% of the solar spectrum. Therefore, the conversion efficiency from solar energy to chemical hydrogen over photocatalysts responsive to UV light is severely limited^[29]. To address this challenge and circumvent the inherent limitations of wide bandgap photocatalysts, several

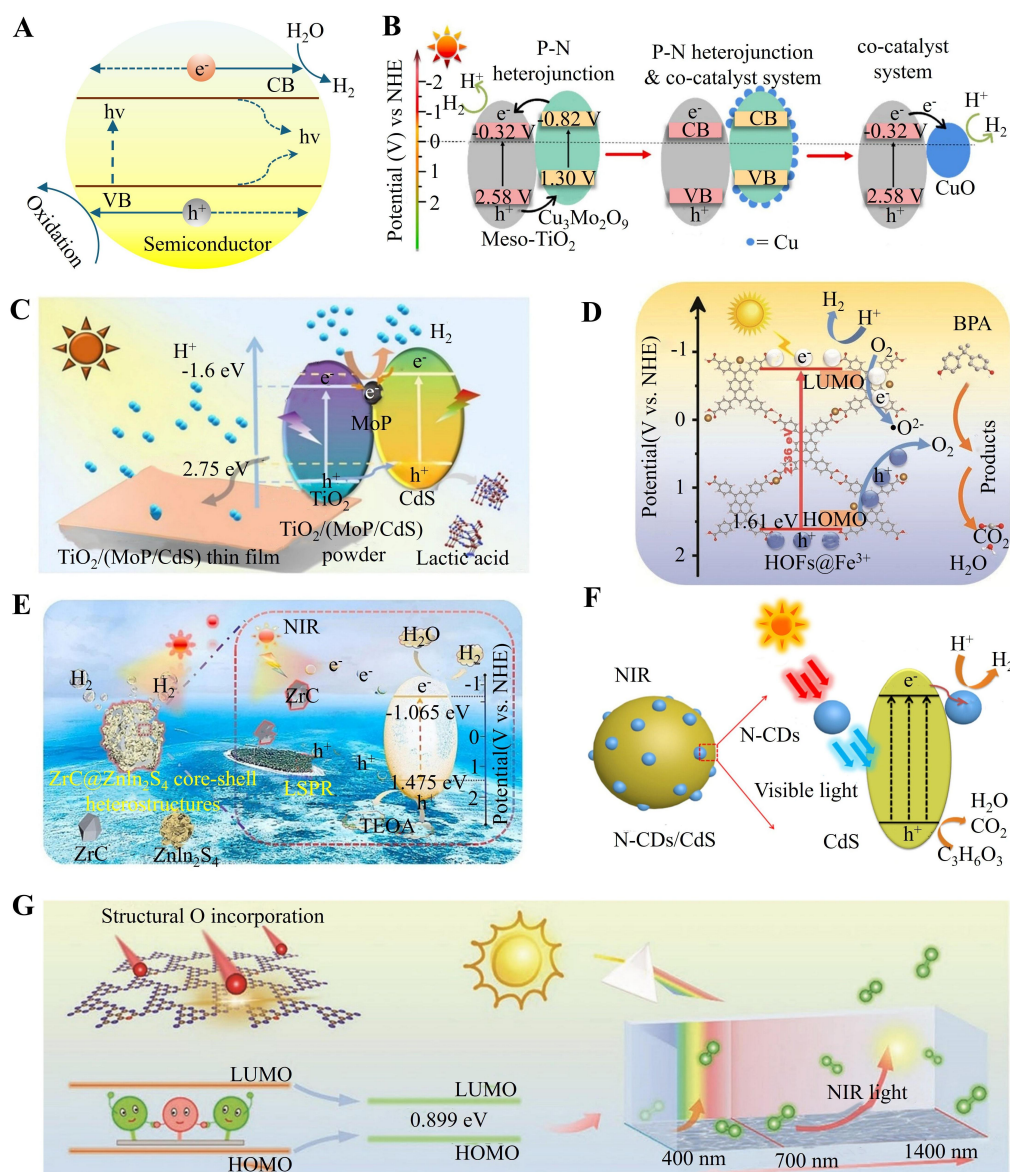


Figure 5. (A) Schematic diagram presenting the principle of photocatalytic hydrogen production; (B) Energy band diagram and charge transfer behavior of $meso-TiO_2/Cu_3Mo_2O_9/CuO$. This figure is quoted with permission from Chen *et al.*^[30]; (C) Schematic diagram elucidating the photocatalytic H_2 production process over $TiO_2/(MoP/CdS)$. This figure is quoted with permission from Wang *et al.*^[32]; (D) Mechanism diagram of $HOFS@Fe^{3+}$ for photocatalytic H_2 production. This figure is quoted with permission from Yang *et al.*^[31]; (E) Schematic diagram of photocatalytic H_2 evolution over $ZrC@ZnIn_2S_4$ core-shell heterostructure upon near-infrared light (NIR) irradiation. This figure is quoted with permission from Shi *et al.*^[29]; (F) Mechanism of photocatalytic H_2 generation over NCDs/CdS. This figure is quoted with permission from Shi *et al.*^[25]; (G) Schematic representation of the structure-performance correlation in MC-CN. This figure is quoted with permission from You *et al.*^[28]. MC-CN: Monomolecular carbonylhydrazide-carbon nitride; ZIS: $ZnIn_2S_4$.

methodologies focusing on enhancing carrier separation and facilitating carrier transfer have been proposed. For example, Chen *et al.* conducted an in-depth investigation into the impact of electron transfer on the photocatalytic hydrogen production performance of composite catalyst $Cu_3@TiO_2$ ^[30]. They demonstrated that the interactions among TiO_2 , copper molybdate, and the newly formed CuO constituted a dual-channel electron transfer system (p-n heterojunction and co-catalyst), which significantly increased the transfer rate of photoexcited electrons, giving access to a high hydrogen evolution rate of $9.6 \mu\text{mol h}^{-1}$ [Figure 5B]. Owing to the restricted solar light utilization efficiency of wide bandgap photocatalysts, UV

light-responsive photocatalysts need to be modified through element doping, defect engineering, or by integration with other narrow bandgap photocatalysts for realizing high-efficient hydrogen production.

Visible-light-responsive photocatalysts

Visible light constitutes approximately 43% of the solar spectrum's energy^[31]. Therefore, the development of photocatalytic materials that can effectively respond to visible light is essential for enhancing photocatalytic efficiency. In this context, various strategies, such as defect engineering, localized surface plasmon resonance, element doping, heterostructure construction, and sensitization, have been proposed to regulate the energy band structure of photocatalysts, and obvious achievements have been witnessed. For example, Wang *et al.* employed a non-precious metal co-catalyst molybdenum phosphide (MOP) to modify TiO₂ and CdS, forming a TiO₂/MOP/CdS film, which was then crafted on polymethyl methacrylate (PMMA) acrylic glass [Figure 5C]^[32]. It exhibited a high photocatalytic hydrogen evolution efficiency of 35.5 mmol g⁻¹ h⁻¹ and long-term stability of up to 150 h under visible light irradiation. Shi *et al.* constructed a hierarchical 1D/2D CoS_{1.097}@ZnIn₂S₄ photocatalyst, where 2D ZnIn₂S₄ nanosheets and 1D flower-like CoS_{1.097} nanoparticles acted as the shell and core, respectively^[29]. The intimate interfacial contact within the structure served as an effective collector for electron transfer, which facilitated the rapid transfer and separation of photogenerated charge carriers and accelerated proton reduction on the surface, consequently enhancing hydrogen production efficiency. Huang *et al.* utilized elemental red phosphorus (RP) to decorate the surface of TiO₂ hollow spheres to broaden the light absorption range of TiO₂, and the obtained TiO₂@RP heterostructure presented a high hydrogen production rate of 215.5 μmol g⁻¹ h⁻¹ under the simulated sunlight irradiation, which is 11.1 times higher than detected over TiO₂^[33]. The increased photocatalytic hydrogen efficiency was attributed to the enhanced light absorption due to the hollow sphere structure and RP photosensitizer and promoted carrier separation caused by the interface heterostructure. These findings demonstrate structure design and heterojunction construction can not only increase light absorption rate but also facilitate carrier separation, leading to strikingly enhanced photocatalytic hydrogen production activity.

Furthermore, to simultaneously address environmental pollution and energy shortage issues through photocatalytic technology, bifunctional catalytic materials are developed. Yang *et al.* constructed a porous nanomaterial (HOFS@Fe³⁺) where non-noble metal ions Fe³⁺ were anchored on nanorod-shaped hydrogen-bonded organic frameworks (HOFS) through electrostatic and coordination interactions [Figure 5D]^[31]. Due to its high specific surface area and abundant hydrogen-bonding adsorption active centers, HOFS@Fe³⁺ was capable of interacting with the bis-OH groups in bisphenol A (BPA), reaching a degradation efficiency of 90%. Furthermore, the ordered conjugated stacking framework structure of HOFS, the hydrogen bonds, and the variable valence nature of Fe³⁺ created an efficient pathway for the separation of photogenerated carriers, resulting in an outstanding photocatalytic hydrogen production efficiency of 21.55 mmol g⁻¹ h⁻¹ under light (λ > 510 nm) irradiation.

Infrared-light-responsive photocatalysts

Infrared light accounts for more than 50% of solar energy, which has long been neglected in the field of photocatalysis due to its low photon energy. Therefore, the development of infrared light-responsive photocatalysts is expected to enhance the quantum efficiency of photocatalytic hydrogen production. In recent decades, several methodologies have been proposed to extend the light absorption range of photocatalysts from UV or visible light to infrared light. These methods include integrating wide-bandgap photocatalysts with upconversion luminescence materials, depositing plasmonic nanoparticles on the surfaces of photocatalysts, and introducing various functional materials, among others.

For example, Shi *et al.*^[29] developed an efficient photothermal auxiliary system $\text{ZrC@ZnIn}_2\text{S}_4$ within a core-shell structure [Figure 5E], where ZrC particles not only prevented the agglomeration of ZnIn_2S_4 nanosheets but also increased the specific surface area and active sites. Upon near-infrared ($\lambda > 800$ nm) irradiation, hot electrons originated from the local surface plasmonic resonance effect of metallic ZrC injected into the conduction band of ZnIn_2S_4 and subsequently participated in water splitting reaction, achieving a hydrogen production rate of $32.87 \text{ mol g}^{-1} \text{ h}^{-1}$. Shi *et al.* designed a low-cost, high-efficiency, and high-stability broadband N-doped carbon dot (N-Cd)/CdS composite^[25]. Its near-infrared photocatalytic activity mainly came from the upconversion photoluminescence characteristics of N-CD, which can upconvert near-infrared light into visible light for achieving photocatalysis, leading to an efficient hydrogen production of $57 \text{ } \mu\text{mol g}^{-1}$ [Figure 5F]. In addition, You *et al.* reported a near-infrared crystalline carbon nitride single photocatalyst using monomolecular carbonyl hydrazine (CBZ) as a precursor, in which structural oxygen introduced from precursor CBZ into the CN framework replaced some edge nitrogen sites. It endowed carbon nitride single photocatalyst with a highly crystalline structure, an elevated charge transfer rate, and a high hydrogen evolution rate of $57 \text{ } \mu\text{mol g}^{-1}$ under the irradiation of infrared light [Figure 5G]^[28]. Although obvious achievements have been made, the development of infrared-light-responsive photocatalysts for high-efficient hydrogen production remains a significant challenge, mainly due to the limited energy conversion efficiency.

Compared to other hydrogen production technologies, photocatalytic technology faces significant challenges in terms of stability and efficiency^[34-36]. These challenges primarily stem from the instability of solar light irradiation, the low energy density of solar energy, and the inadequate stability and efficiency of photocatalysts. The low efficiency of photocatalytic hydrogen evolution can be primarily attributed to inadequate light energy capture, suboptimal charge carrier dynamics, and insufficient surface reaction efficiency. These issues stem from a narrow absorption spectrum and low energy utilization efficiency, rapid recombination of photogenerated electron-hole pairs, and inappropriate energy band positions, respectively. To address these challenges, several strategies can be employed. From a material science perspective, band engineering and microstructure design are crucial to broadening the spectral response range. Introducing gradient energy levels or built-in electric fields within photocatalysts is desired to facilitate the directed separation of charge carriers. Surface modification with co-catalysts or the creation of atomic-level active sites is a promising modulation strategy to lower the reaction energy barrier, accelerate proton adsorption and reduction processes, and inhibit reverse reactions by establishing selective transport pathways. Furthermore, the enhanced stability of photocatalysts can be achieved by optimizing the catalyst surface passivation layer or designing core-shell structures to protect against electrolyte corrosion. Additionally, coupling photothermal synergistic effects or employing external electric field assistance can improve overall energy conversion efficiency. Developing dynamic monitoring methods enables real-time adjustment of reaction conditions, balancing the effects of light intensity, temperature, and mass transfer on hydrogen production performance. By integrating these approaches, the efficiency, stability, and scalability of photocatalytic hydrogen production can be significantly improved, paving the way for more sustainable and economically viable hydrogen generation technologies.

PHOTOELECTROCATALYTIC HYDROGEN PRODUCTION

Basic principle of photoelectrocatalytic hydrogen evolution

Photoelectrocatalysis is a process that occurs under the simultaneous influence of light radiation and an applied bias voltage^[37-41]. As displayed in Figure 6A, under the irradiation of light with photon energy greater than or equal to the bandgap energy of the semiconductor, the electrons of semiconductor photocatalyst (photoelectrode) in the VB are excited to the CB, forming photogenerated electron-hole pairs. The photoexcited electrons and holes are spatially separated and transferred toward the edge of the CB and VB, respectively, driven by the applied bias voltage. Subsequently, the separated electrons and holes migrate

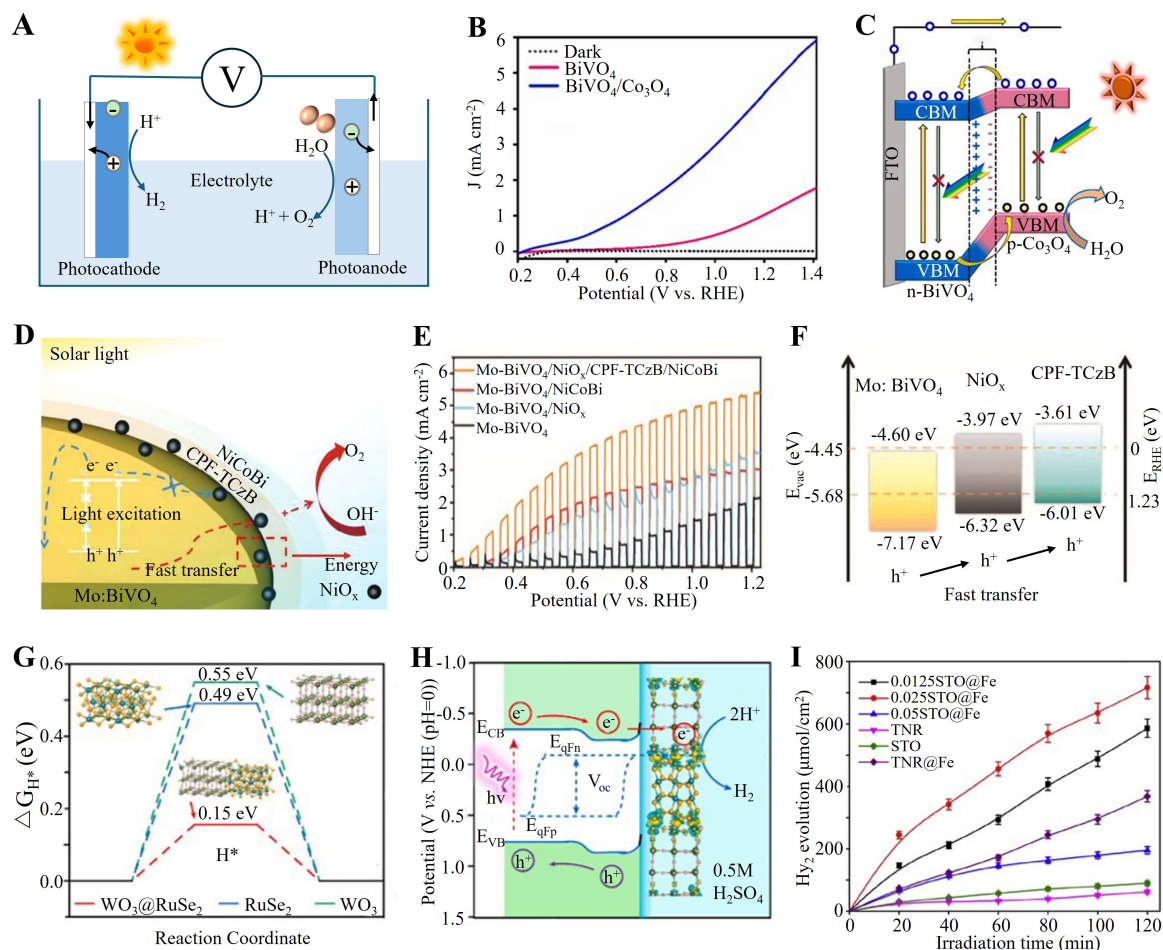


Figure 6. Photoelectrocatalytic hydrogen production. (A) Schematic representation of the principle of photoelectrocatalysis; (B) LSV curves obtained for BiVO_4 and $\text{BiVO}_4/\text{Co}_3\text{O}_4$ in 0.5 M Na_2SO_4 under dark and light illumination; (C) Schematic illustration of charge transfer within $\text{BiVO}_4/\text{Co}_3\text{O}_4$ p-n junction photoanode during overall photoelectrocatalytic water splitting. Figure B and C are quoted with permission from Murugan et al.^[44]; (D) Schematic diagram of photoelectrocatalytic water splitting over $\text{Mo:BiVO}_4/\text{NiO}_x/\text{CPF-TCzB}/\text{NiCoBi}$; (E) PEC performance of different samples; (F) Energy band diagrams of Mo:BiVO_4 , NiO_x , and CPF-TCzB . Figure D-F are quoted with permission from Wang et al.^[45]; (G) Gibbs free energy for hydrogen generation over the $\text{n}^+\text{-p-Si}/\text{Ti}/\text{WO}_3/\text{RuSe}_2$, $\text{n}^+\text{-p-Si}/\text{Ti}/\text{RuSe}_2$, $\text{n}^+\text{-p-Si}/\text{Ti}/\text{WO}_3$, and bare $\text{n}^+\text{-p-Si}/\text{Ti}$; (H) Possible E_0 optimization mechanism (E_{CB} : conduction band, E_{VB} : valence band). Figure G and H are quoted with permission from Zhang et al.^[46]; (I) Hydrogen production over fabricated STO@Fe NR photocatalyst with different concentrations of Sr. This figure is quoted with permission from Bashiri et al.^[47]. LSV: Linear sweep voltammetry; PEC: photoelectrochemical.

to the surface of the semiconductor and exclusively flow through an external circuit to the cathode and remain on the surface of the photoanode. As a consequence, holes participate in oxidation reactions (oxidizing water into oxygen and protons) at the photoanode, and electrons take part in reduction reactions (reducing protons into hydrogen) at the cathode. Compared with photocatalysis, photoelectrocatalytic hydrogen production demonstrates superior stability and efficiency as a result of enhanced carrier separation and transfer. The primary chemical reactions occurring during photoelectrocatalytic hydrogen production can be described by the following equations:



Oxidation reaction (OER, photoanode surface):

Acidic conditions: $2\text{H}_2\text{O} + 4h^+ \rightarrow \text{O}_2 \uparrow + 4\text{H}^+$ ($E_o = 1.23$ V vs. RHE);

Alkaline conditions: $4\text{OH}^- + 4h^+ \rightarrow \text{O}_2 \uparrow + 2\text{H}_2\text{O}$ ($E_o = 0.40$ V vs. RHE);

Reduction reaction (HER, cathode surface):

Acidic conditions: $2\text{H}^+ + 2e^- \rightarrow \text{H}_2 \uparrow$ ($E_o = 0$ V vs. RHE);

Alkaline conditions: $2\text{H}_2\text{O} + 2e^- \rightarrow \text{H}_2 \uparrow + 2\text{OH}^-$ ($E_o = -0.83$ V vs. RHE);

Total reaction (water splitting): $2\text{H}_2\text{O} \rightarrow 2\text{H}_2 \uparrow + \text{O}_2 \uparrow$ ($\Delta G_o = +237.1$ kJ/mol).

Recent advancements in photoelectrocatalytic hydrogen production

The development of photoelectrocatalytic hydrogen evolution is intricately linked to photocatalytic and electrocatalytic hydrogen production technologies^[42], encompassing mechanism elucidation, material characterization, and practical implementation. Photoelectrocatalytic hydrogen production demonstrates more superior stability and efficiency than photocatalysis, which is resulted from the enhanced carrier separation and transfer rates in the presence of bias voltage. Compared to electrocatalysis, photoelectrocatalytic hydrogen production requires a lower input of electrical energy, offering a more sustainable approach to hydrogen generation. Consequently, this field has garnered increasing attention, leading to the development of numerous advanced photoelectrocatalytic materials and systems, which can be classified into two categories according to the utilization of the applied electric source, routine and self-driven photoelectrocatalytic hydrogen production systems. Some typical representatives are summarized in Table 1.

Routine photoelectrocatalytic hydrogen production system

Photoelectrocatalytic materials with heterojunction structures demonstrate superior performance in energy band modulation^[43], enhanced carrier separation and migration, expanded light absorption spectrum, and increased active sites compared to single-component catalysts, leading to improved hydrogen production efficiency. For example, Murugan *et al.* constructed $\text{BiVO}_4/\text{Co}_3\text{O}_4$ photoanode to realize photoelectrocatalytic hydrogen evolution through a simple yet robust pulsed laser deposition method. The results indicated that the photocurrent density of 4.66 mA cm^{-2} with the overpotential of $+1.23$ V was observed over the $\text{BiVO}_4/\text{Co}_3\text{O}_4$ photoanode, which was 4 times that of the original BiVO_4 photoanode [Figure 6B]. They attributed the enhanced photoelectrocatalytic performance to the contact interface formed within the p-n junction between Co_3O_4 and BiVO_4 [Figure 6C]^[44]. Wang *et al.* developed an efficient photoelectrochemical water-splitting photoanode comprised of $\text{Mo:BiVO}_4/\text{NiOx}/\text{CPF-TCzB}/\text{NiCoBi}$ [Figure 6D], which showcased much higher photocurrent density (5.40 mA cm^{-2}) at 1.23 V vs. RHE upon 0.5 M phosphate buffer solution and 1.5 AM light irradiation (100 mW cm^{-2}) than those detected over Mo:BiVO_4 (2.15 mA cm^{-2}), $\text{Mo:BiVO}_4/\text{NiOx}$ (3.53 mA cm^{-2}), and $\text{Mo:BiVO}_4/\text{NiCoBi}$ (3.00 mA cm^{-2}) in the presence of NiOx and CPF-TCzB [Figure 6E]^[45]. As presented in Figure 6F, an energy level gradient was established within $\text{Mo:BiVO}_4/\text{NiOx}/\text{CPF-TCzB}/\text{NiCoBi}$, which played a vital role in eliminating the potential barrier between BiVO_4 and $\text{NiOx}/\text{CPF-TCzB}$. The decreased energy level difference within the composite catalyst facilitated the transport of photogenerated holes from Mo:BiVO_4 to the co-catalyst $\text{NiOx}/\text{CPF-TCzB}$, and undesirable interfacial charge recombination was effectively suppressed. These findings highlight the critical importance of constructing a compact interface with suitable energy level

differences in heterojunction photoelectrocatalysts to enhance charge separation and transfer, thereby significantly improving hydrogen production performance.

Zhang *et al.* developed a high-performance photocathode heterostructure system for solar $\text{WO}_3/\text{RuSe}_2$ hydrogen evolution, which showcased a short-circuit photocurrent density of 36 mA cm^{-2} and a half-cell solar hydrogen conversion efficiency of 9.43%^[46]. To get deep insight into the obvious photoelectrocatalytic performance, theoretical simulation calculation centering on the hydrogen generation reaction pathway was performed. The calculated result is displayed in Figure 6G. It indicated that Gibbs free energy for H^+ adsorption over $\text{WO}_3/\text{RuSe}_2$ (0.15 eV) was much lower than that observed over pristine WO_3 and RuSe_2 , implying the more superior capability of $\text{WO}_3/\text{RuSe}_2$ in hydrogen production. Based on this, a possible hydrogen generation pathway was proposed, as depicted in Figure 6H. In detail, the charge redistribution between p-Si and heterostructure $\text{WO}_3/\text{RuSe}_2$ facilitated the bending of the d-band center of $\text{WO}_3/\text{RuSe}_2$ heterostructure toward the Fermi level, enabling H^+ adsorption. This significantly inhibited the interfacial charge recombination, thereby improving overall efficiency. In addition, Bashiri *et al.* developed a layered modified $\text{SrTiO}_3/\text{TiO}_2/\text{Fe}_2\text{O}_3$ nanorod heterostructure, which exhibited a maximum photocurrent density of 0.63 mA cm^{-2} and a photoconversion efficiency of 0.69%, leading to the highest hydrogen production rate of $716 \mu\text{mol cm}^{-2}$ under visible light irradiation [Figure 6I]^[47]. The enhanced hydrogen evolution performance was attributed to the efficient separation of electrons and holes in a wide-narrow bandgap composite catalyst system. These results further demonstrate that the heterojunction structure featuring a built-in electric field and a broad light absorption range is beneficial for improving carrier separation and light utilization, thereby boosting catalytic hydrogen production efficiency.

Self-driven photoelectrocatalytic hydrogen production

Photovoltaic devices and nanogenerators present an innovative approach to hydrogen production, wherein the bias voltage required for photoelectrocatalytic hydrogen evolution is self-generated under light irradiation, eliminating the need for an external power supply. The first kind of self-driven photoelectrocatalytic hydrogen production system consists of two main devices, photovoltaic cell and electrolyzer, in which the electricity generated by the photovoltaic cell drives the water splitting reaction in the electrolyzer under light irradiation. Furthermore, the second type of self-driven photoelectrocatalytic hydrogen production system utilizes piezoelectric, pyroelectric, or triboelectric nanogenerators to supply electricity and drive water splitting reactions at the electrode surface under light irradiation.

Based on the first kind of hydrogen production system, Kim *et al.* developed a hetero-tandem organic optoelectronic device consisting of large (PM6:IT-M) and small bandgap (PM6:Y6) bulk heterojunctions, which presented an open-circuit voltage of 1.84 V and short current of 9.81 mA cm^{-2} , achieving an outstanding power conversion efficiency of 11.7% [Figure 7A]^[48]. Notably, when the fabricated organic optoelectronic device was integrated with an alkaline electrolyzer comprising $\text{NiFeO}_x(\text{OH})_y$ and Pt (functioning as the oxygen evolution catalyst and hydrogen evolution catalyst), remarkable solar-to-hydrogen and electricity-to-hydrogen conversion efficiencies of 10% and 84.5% were achieved, respectively. Seo *et al.* proposed a stable and efficient organic semiconductor-based photoelectric cell photocathode [Figure 7B], which retained over 95.4% of its peak photocurrent for more than 30 h, without significant degradation observed in the organic semiconductor. The developed photoelectrode system showcased a large-scale hydrogen production yield of about 3500 ppm in 120 min under daylight irradiation [Figure 7C]^[49].

As for the second type of hydrogen production system, Gong *et al.*^[50] fabricated an integrated system consisting of triboelectric nanogenerator (TENG) and electrochemical reactor, which was capable of

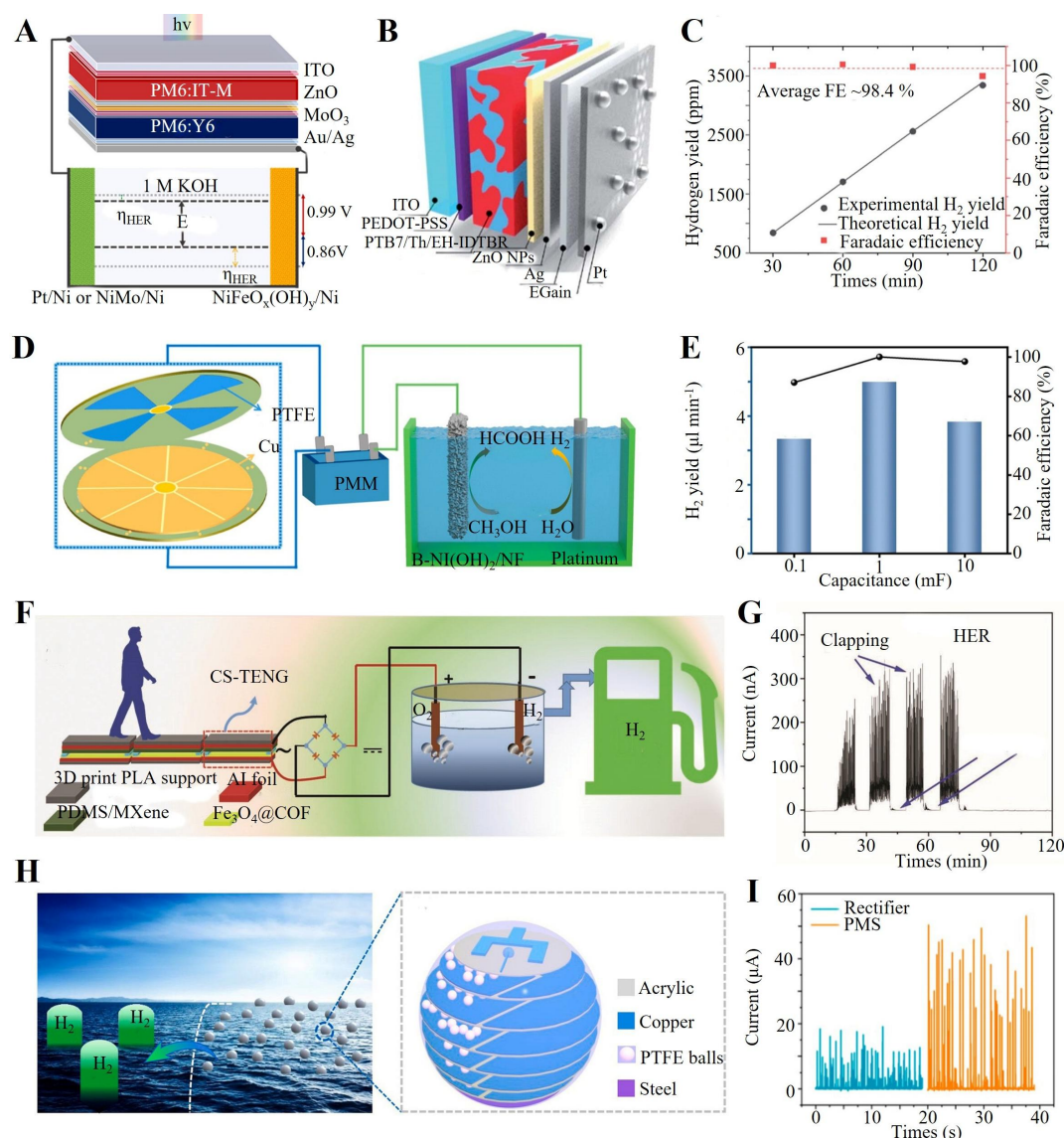


Figure 7. Self-driven photoelectrocatalytic H₂ production. (A) Schematic representative of the organic optoelectronic device for H₂ evolution. This figure is quoted with permission from Kim *et al.*^[48]; (B) Schematic structure illustration of PTB7-Th/EH-IDTBR photocathode and (C) the corresponding H₂ evolution rate. Figure A-C are quoted with permission from Bashiri *et al.*^[47]; (D) Schematic diagram of the UDC RF-Pulsed-TENG system, and (E) the corresponding H₂ generation rate and Faraday efficiency. Figure D and E are quoted with permission from Gong *et al.*^[50]; (F) Illustration of biomechanical energy conversion into H₂ fuel based on the integrated CS-TENG and electrochemical reactor, and (G) the continuous clapping converted into electricity for H₂ evolution. Figure F and G are quoted with permission from Ghosh *et al.*^[51]; (H) Schematic diagram of the structure of ID-TENG, and (I) the corresponding short-circuit current output of ID-TENG connecting to PMS and bridge rectification. Figure H and I are quoted with permission from Zhang *et al.*^[52]. PMS: Power management system; ID-TENG: instant discharging triboelectric nanogenerator.

generating green hydrogen at the cathode and formic acid at the anode driven by unidirectional current-induced rotational-independent triboelectric layer mode pulses [Figure 7D]. Significantly, compared with the traditional switching transformer power supply management method, the green hydrogen production rate (4.99 μL min⁻¹) was increased by about 1.68 times [Figure 7E]. Ghosh *et al.* utilized magnetic covalent organic framework composites as the positive triboelectric material in a contact-separation mode triboelectric nanogenerator (CS-TENG), which was integrated with an electrochemical reactor, forming a self-driven photoelectrocatalytic hydrogen production system

[Figure 7F]. The constructed system achieved efficient energy conversion from mechanical energy from human motion into electrical energy, which was subsequently used for water splitting to produce hydrogen [Figure 7G]^[51]. In addition, Zhang *et al.* proposed a multilayer bead self-powered hydrogen production system that combines spherical TENG with a power management system (PMS) [Figure 7H]. The trigger switch utilized in the ball mechanism employed an instantaneous drive system to overcome the limitations associated with operating frequency, thereby significantly enhancing output performance. The integrated TENG was capable of charging a 470 μF capacitor to 5 V by efficiently converting water wave energy into electrical energy, which split water into hydrogen with a notable rate of approximately $64.5 \mu\text{L min}^{-1}$ [Figure 7I]^[52]. The studies strongly demonstrated that efficient hydrogen production can be realized under the stimulation of light irradiation and environmental low-density energy, such as human motion, water waves, wind, sound waves, and so on, based on the integration of electrochemical reactor and nanogenerators.

Compared to photocatalysis and electrocatalysis, photoelectrocatalytic hydrogen production technology offers significant advantages, including enhanced carrier separation efficiency and reduced reliance on external energy inputs^[50]. Despite its promise, several challenges hinder the large-scale practical application of this technology. A primary issue is the multidimensional mismatch between light absorption, charge separation, and surface reaction kinetics. The limited light response range of semiconductor materials restricts the generation of sufficient photogenerated charge carriers, while the high rate of charge recombination in bulk and at interfaces far exceeds the effective migration rate, resulting in substantial energy loss as heat. Furthermore, the lack of bifunctional catalytic activity at the electrochemical interface significantly limits overall efficiency. Additionally, photoelectrodes are susceptible to photo-corrosion or structural degradation under the combined stresses of intense light exposure, electrolyte corrosion, and applied bias, making it difficult to achieve the long-term operational stability required for practical applications. To overcome these challenges, several strategies can be employed. For instance, designing gradient band structures or constructing heterojunctions can broaden the spectral absorption range and create built-in electric fields to facilitate the separation of photogenerated electrons and holes. Modulating atomic-level active sites can lower the energy barrier for surface reactions, while introducing selective transport layers can suppress side reactions, thereby improving charge transfer efficiency between the photoelectrode and the electrolyte. Moreover, constructing conductive protective layers or adaptive passivation films can enhance corrosion resistance without compromising catalytic activity. Optimizing the multi-field coupling mechanisms of light, electricity, and heat, starting from the intrinsic fatigue resistance of materials, can provide insights into lifespan prediction and failure protection strategies through advanced multiscale simulation and modeling. By integrating these approaches, the efficiency, stability, and scalability of photoelectrocatalytic hydrogen production would be significantly improved.

SYNERGISTIC CATALYTIC HYDROGEN PRODUCTION

Synergistic catalytic hydrogen production is the coupling among different catalysis, which can be classified into piezo-pyrocatalysis, piezo-photocatalysis, pyro-photocatalysis, and piezo-pyro-photocatalysis. In contrast to one specific catalysis, synergistic catalytic hydrogen production offers more advantages in terms of efficiency, flexibility, energy utilization efficiency, economic viability, and environmental adaptability. The recent advancements in the above-mentioned synergistic catalysis for hydrogen production will be exclusively discussed below.

Piezo-pyrocatalytic hydrogen production

To achieve synergistic hydrogen production through the integration of piezocatalysis and pyrocatalysis, it is crucial to develop ferroelectric catalytic materials that exhibit spontaneous polarization along with high

sensitivity to both applied mechanical stress and temperature variations. In this process, environmental mechanical and thermal energy can be harnessed to split water into hydrogen, with the efficiency of hydrogen production being highly dependent on the piezoelectric and pyroelectric potential outputs. From this perspective, strategies aimed at enhancing the piezoelectric and pyroelectric properties are essential for improving the performance of piezo-pyrocatalytic hydrogen production. Therefore, the crystallographic orientation within the piezo-pyrocatalyst, a critical factor that determines the piezoelectric and pyroelectric responses to applied mechanical and thermal stimuli, the electron transfer pathways during catalytic reactions and the exposure of active sites, must be precisely controlled to achieve highly efficient hydrogen evolution^[53–55]. For example, Zhang *et al.* proposed that the crystallographic orientation of hexagonal-phase CdS, governed by its non-centrosymmetric structure (space group P63mc), critically dictated its spontaneous polarization behavior, and thus impacted its pyroelectric effect under thermal fluctuations^[26]. Previous studies have shown that surface modification of piezo-pyrocatalysts significantly enhanced interfacial charge transfer efficiency, resulting in an increased hydrogen evolution rate. Therefore, a rational material design approach integrating structural considerations with interfacial modifications to enhance thermoelectric conversion efficiency and catalytic activity is highly desirable.

Despite its promising potential, the investigation of piezo-pyrocatalytic technology remains in its infancy^[56], primarily owing to the intrinsic limitations of available materials. On one hand, the intricate coupling mechanism between piezoelectricity and pyroelectricity remains unclear, which poses significant challenges in optimizing the composition, crystal structure, and phase structures of ferroelectric catalysts. On the other hand, the development of theoretical simulation calculations for the coupling among mechanical force, temperature fluctuations, piezoelectricity, and pyroelectricity lacks depth, thereby limiting its ability to guide the exploration and optimization of conditions for achieving highly efficient synergistic piezo-pyrocatalytic hydrogen production. Therefore, significant efforts should be devoted to both experimental and theoretical investigations of synergistic piezo-pyrocatalytic hydrogen production. The development of advanced ferroelectric catalysts and piezocatalytic-pyrocatalytic composites is critically required.

Piezo-photocatalytic hydrogen production

Piezo-photocatalytic hydrogen production can be achieved over piezoelectric photocatalytic semiconductor or piezoelectric-photocatalytic composites under the stimuli of mechanical stress and light irradiation^[57]. From the perspective of energy band theory, as depicted in Figure 8A^[58], the piezoelectric field formed at the ideal interface between the piezoelectric material and photocatalyst induces either upward or downward energy band bending. This phenomenon, driven by the piezo-phototronic effect, further optimizes carrier separation and transfer dynamics, consequently boosting the efficiency of photocatalytic hydrogen evolution. Specifically, when subjected to simultaneous light irradiation and mechanical strain, a piezoelectric field is generated on the surface of the piezoelectric material. This field acts as a potent driving force, directing photoexcited electrons and holes to migrate in opposite directions, thereby significantly enhancing carrier separation and transfer efficiency [Figure 8B]. Moreover, the induced piezoelectric field not only enhances photocatalytic activity but also enables piezocatalytic hydrogen production through the piezocatalysis mechanism. Consequently, compared to standalone piezocatalytic or photocatalytic hydrogen production technologies, the integrated piezo-photocatalytic approach demonstrates superior performance in terms of energy conversion efficiency, owing to the synergistic interplay between these two catalytic mechanisms.

Based on the above merits of piezo-photocatalysis, plenty of piezo-photocatalysts have been developed. For example, Wang *et al.*^[59] prepared barium strontium titanate ($\text{Ba}_{0.7}\text{Sr}_{0.3}\text{TiO}_3$) nanorod arrays (BST NRs) on a glass substrate as a recoverable catalyst for investigating their piezo-photocatalytic hydrogen production

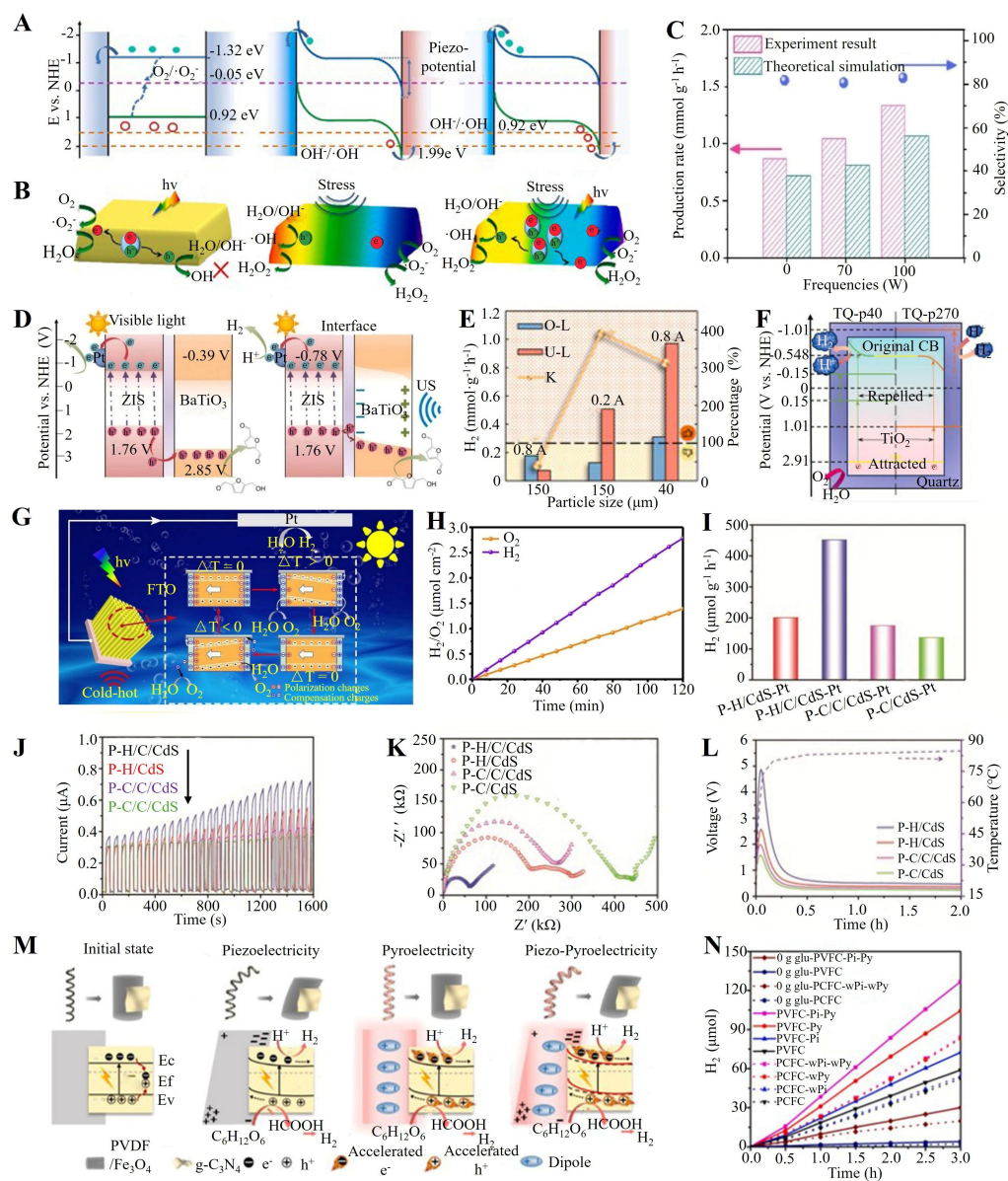


Figure 8. Synergistic catalysis for H_2 production. Schematic diagram of (A) energy band bending of catalyst and (B) carrier behavior within catalyst during piezo-photocatalysis. Figure A and B are quoted with permission from Han et al. [58]; (C) Experimental and simulated piezo-photocatalytic H_2 production rate and selectivity of Pt/ ZnIn_2S_4 /BaTiO₃ heterojunctions, and (D) corresponding H_2 production mechanism. Figure C and D are quoted with permission from Wang et al. [59]; (E) Schematic illustration of the piezopotential switch mechanisms, and (F) corresponding H_2 production rates under ultrasonication-light (U-L) and stirring-light irradiation (O-L) with the working current of 0.8 and 0.2 A, respectively. Figure E and F are quoted with permission from Jin et al. [61]; (G) Schematic representative of the synergistic pyro-photocatalytic water splitting over BaTiO₃ photoanode, and (H) corresponding H_2/O_2 production under temperature fluctuation, light illumination, and an overpotential of 1.23 V vs. RHE. Figure G and H are quoted with permission from Guo et al. [63]; (I) Hydrogen evolution rates, (J) electrochemical impedance spectroscopy Nyquist plots, (K) photocurrent outputs, and (L) pyroelectric potential outputs of P(VDF-HFP)/CNT/CdS-Pt (P-H/C/CdS-Pt), P(VDF-HFP)/CNT/CdS-Pt (P-H/C/CdS-Pt), P(VDF-CTFE)/CNT/CdS-Pt (P-C/C/CdS-Pt), and P(VDF-HFP)/CNT/CdS-Pt (P-C/CdS-Pt). Figure I-L are quoted with permission from Dai et al. [7]; (M) Schematic representation of piezo-pyro-photocatalytic H_2 production in the condition of magnetic field stimulation, full-spectrum light irradiation, and (N) corresponding H_2 production rates of PVDF/ Fe_3O_4 /g-C₃N₄ (PVFC). Figure M and N are quoted with permission from Wei et al. [64]. RHE: Reversible hydrogen electrode; PVDF: polyvinylidene fluoride.

performance. The results suggested that the hydrogen generation efficiency of polarized BST NRs observed under light irradiation in the presence of ultrasonic vibration (411.5 mmol g⁻¹ h⁻¹) was 1.7 times higher than

that in the absence of ultrasonic vibration (photocatalysis), strongly demonstrating the significance of synergistic piezo-photocatalysis for efficient hydrogen production^[60]. In addition, Yang fabricated a novel piezo-photocatalyst platinum/zinc indium sulfate barium (Pt/ZIS/BaTiO₃) with a unique one-dimensional/two-dimensional core-shell structure to further improve piezo-photocatalytic hydrogen production performance, and a high hydrogen evolution rate of 1,335.3 $\mu\text{mol g}^{-1} \text{h}^{-1}$ and a theory simulation generation rate of 1,070.8 $\mu\text{mol g}^{-1} \text{h}^{-1}$ under light irradiation and ultrasonic vibration were observed, which are much higher than that obtained over pristine ZIS [Figure 8C]^[59]. The strikingly enhanced piezo-photocatalytic hydrogen production rate was attributed to the internal BaTiO₃ serving as a hole-storage layer, the external Pt nanoparticles acting as electron capture centers, and the piezoelectric field generated within the constructed unique structure, which played a significant role in facilitating carrier separation [Figure 8D].

Furthermore, Jin *et al.* studied the impact of piezoelectric potential generated by quartz/TiO₂ particles of different sizes under ultrasonic vibration on hydrogen production efficiency through experiments and COMSOL simulation^[61]. Specifically, the hydrogen production enhancement factor (the ratio of hydrogen production rate under the combined influence of ultrasound and light to that under light alone) was significantly increased over quartz/TiO₂ when the size of quartz was decreased from 150 (with a potential output of 1.125 V) to 40 μm (corresponding to 0.3 V) upon the working current of 0.8 A [Figure 8E]. They attributed this phenomenon to the fact that the weak piezoelectric potential (< 1 V) played a positive role in enhancing piezo-photocatalytic hydrogen production performance by promoting the separation of photogenerated charge carriers [Figure 8F]. Conversely, the strong piezoelectric potential (> 1 V) caused the energy bands to bend downwards, reducing the electron reduction capability and thus inhibiting hydrogen production^[60]. Moreover, a notably increased hydrogen production enhancement factor of 3.9 was achieved over 150 μm quartz/TiO₂ sample under the working current of 0.2 A, which was much 10 times higher than detected under 0.8 A [Figure 8E], further demonstrating the modulation role of piezoelectric potential in adjusting piezo-photocatalytic hydrogen evolution performance. This study corroborated that the hydrogen production efficiency was predominantly determined by the piezoelectric potential output, which was significantly dependent on the grain size of piezoelectric quartz and working currents. Therefore, it is necessary to optimize the grain size and piezoelectric property of piezoelectric component within piezo-photocatalysts for achieving high-efficient hydrogen production.

Pyro-photocatalytic hydrogen production

Pyro-photocatalytic synergistic hydrogen production process can be achieved over pyroelectric photocatalyst or pyroelectric-photocatalytic composite materials under the co-stimulation of light irradiation and temperature fluctuations, and the pyro-photocatalytic hydrogen production efficiency is predominately modulated by the pyroelectric and photocatalytic properties of the catalyst. The fundamental principle of pyro-photocatalysis is analogous to that of piezo-photocatalysis, with the key difference being that the mechanical strain stimulus is replaced by temperature fluctuations. To achieve high-performance pyro-photocatalytic hydrogen production, it is necessary to optimize the composition of pyro-photocatalyst and the stimuli conditions^[62], especially for temperature fluctuations. Thakur *et al.* constructed the pyroelectric photocatalytic semiconductor BaTiO₃ and investigated its pyro-photocatalytic hydrogen production efficiency [Figure 8G]^[57]. The results indicated that under the stimulation of hot-cool thermal cycles and light irradiation, an efficient overall water splitting reaction with a stoichiometric ratio of 2:1 between H₂ and O₂ was achieved, demonstrating the great potential of pyro-photocatalysis in hydrogen production [Figure 8H].

To realize self-driven synergistic pyro-photocatalytic hydrogen evolution, Dai *et al.*, for the first time, constructed a photothermal-pyroelectric-photocatalytic multifunctional composite fiber Polyvinylidene fluoride-hexafluoropropylene/carbon nanotube/CdS (PVDF-HFP/CNT/CdS)^[7]. In this structure, the photothermal material CNT that was responsive to infrared light was heated under full-spectrum irradiation, and subsequently heated the pyroelectric material PVDF-HFP, generating a pyroelectric field on the surface. This pyroelectric field not only caused pyrocatalytic hydrogen evolution but also facilitated the separation and transfer of photoexcited carriers in CdS through the pyro-phototronic effect. As a result, an obviously boosted hydrogen evolution rate of $755 \mu\text{mol g}^{-1} \text{h}^{-1}$ with the highest apparent quantum yield of 16.9% was achieved, which was about 5 times higher than observed from photocatalysis [Figure 8I]. To gain deep insight into the carrier behavior during the pyro-photocatalytic hydrogen evolution process, they conducted transient photoelectrochemical characterizations [Figure 8J and K]. The photocurrent results indicated that PVDF-HFP/CNT/CdS sample showed the highest photocurrent value ($0.75 \mu\text{A}$), which was 3 times higher than the photocurrent at room temperature, implying the boosted carrier separation efficiency and migration rates of CdS in the presence of pyroelectric field. Moreover, transient electrochemical impedance spectroscopy [Figure 8K], pyroelectric potential output [Figure 8L], and transient temperature-dependent photoluminescence spectra measurements confirmed that the pyroelectric field significantly enhanced the migration of photogenerated electrons and holes in opposite directions, facilitating carrier transfer, prolonging carrier lifetime, and consequently increasing hydrogen production efficiency. These findings demonstrate that high-efficient synergistic pyro-photocatalytic hydrogen production can be realized by reasonably designing multifunctional materials, and the introduction of photothermal materials is beneficial for full-spectrum solar light utilization.

Piezo-pyro-photocatalytic hydrogen production

By coupling the piezoelectric, pyroelectric, and photocatalytic effects, hydrogen production can be achieved in the conditions of mechanical stress^[59], temperature fluctuation, and light irradiation^[63]. In this process, three types of energy sources are utilized for hydrogen evolution, which will greatly increase the energy conversion efficiency from natural energy to chemical counterpart. In addition, the piezoelectric field and/or pyroelectric field generated on the interface between photocatalyst and piezocatalyst and/or pyrocatalyst will serve as a driving force to promote the separation and transfer of photoexcited carriers, leading to facilitated hydrogen production rate. The basic principles of piezo-pyro-photocatalysis are similar to those of piezo-photocatalysis, both regulating the separation and reaction activity of photogenerated charge carriers through the formation of an internal polarized electric field within the material. Notably, the external excitation conditions for them are different. Piezo-photocatalysis relies on mechanical stress to induce the piezoelectric effect, generating an internal electric field, while piezo-pyro-photocatalysis further introduces temperature fluctuations as an additional stimulus. This is achieved through the coupling of the pyroelectric effect and the piezoelectric effect, enhancing the accumulation and distribution regulation of polarized charges. Under the synergistic excitation of temperature changes and mechanical stress, the asymmetric polarized charges within the material can form a dynamically superimposed spatial electric field, whose intensity and direction adjust dynamically with external thermal-mechanical conditions. This allows for more efficient directional migration of photogenerated electrons and holes, suppressing recombination losses. This multi-physical field coupling mechanism not only broadens the dimensions of energy input (mechanical energy, thermal energy, optical energy) but also optimizes the spatial distribution of charge carriers and surface reaction pathways through dynamic modulation of the electric field, theoretically breaking through the limitations of catalytic efficiency imposed by a single physical field.

Based on the above merits, Wei *et al.* constructed magnetically driven PVDF/ Fe_3O_4 @g- C_3N_4 helical micromotors to facilitate the synergistic coupling among piezoelectric, pyroelectric, and photocatalytic effects for hydrogen evolution [Figure 8M]^[64]. Their results corroborated that under the

stimuli of the magnetic field, helical micromotors rotated periodically and thus formed piezoelectric charges on the surface of PVDF fiber, enabling a piezocatalytic hydrogen evolution rate of $72.4 \text{ mmol g}^{-1} \text{ h}^{-1}$. Under the temperature fluctuations ranging from 40°C to 60°C , pyroelectric charges were formed over PVDF fiber, which led to a pyrocatalytic hydrogen evolution rate of $104.4 \text{ mmol g}^{-1} \text{ h}^{-1}$. Upon light irradiation, a hydrogen evolution rate of $30.1 \text{ mmol g}^{-1} \text{ h}^{-1}$ was achieved over $\text{Fe}_3\text{O}_4@\text{g-C}_3\text{N}_4$. Notably, $\text{PVDF/Fe}_3\text{O}_4@\text{g-C}_3\text{N}_4$ helical micromotors exhibited an outstanding hydrogen production efficiency of $126.7 \text{ mmol g}^{-1} \text{ h}^{-1}$ in the presence of magnetic field, temperature fluctuations, and light irradiation, which was much higher than the hydrogen evolution rate observed over single catalytic pathway [Figure 8N]. The enhanced hydrogen production performance was attributed to the synergistic effect among piezocatalytic, pyrocatalytic and photocatalytic processes, as well as the modulation of piezoelectric and pyroelectric fields on the separation and transfer behavior of photoexcited carriers of photocatalyst. These findings underscore the pivotal role of synergistic catalysis in enhancing hydrogen production performance, positioning it as a focal point in the field of hydrogen production^[65,66].

SUMMARY AND OUTLOOK

In summary, hydrogen, characterized by its high energy density, zero carbon dioxide emissions, and environmentally friendly attributes, is considered a promising alternative to traditional fossil fuels, and the development of efficient hydrogen production technology is of great significance for realizing a hydrogen economy in the future. In this context, this review systematically scrutinized the recent advancements in electrocatalytic, piezocatalytic, pyrocatalytic, photocatalytic, photoelectrocatalytic, and their synergistic catalytic hydrogen production processes. The discussion focuses on fundamental principles, catalyst material composition, structural design, functional engineering, energy utilization efficiency, and carrier behavior modulation, among other aspects. Furthermore, the relationships and distinctions between the aforementioned catalytic hydrogen production processes are explored, which would provide theoretical insights and experimental guidance for the beginner in the field of catalytic hydrogen production.

Despite significant progress in the investigation of catalytic mechanisms and the exploration of catalysts, numerous challenges persist in both the theoretical research and practical implementation of hydrogen production. At first, despite the significant potential of synergistic catalysis in enhancing hydrogen production, the underlying mechanisms of piezo-pyrocatalysis, piezo-photocatalysis, pyro-photocatalysis, and piezo-pyro-photocatalysis remain poorly understood. For instance, the coupling mechanism between pyroelectric polarization charges and piezoelectric polarization charges requires investigation. It is important to examine whether there is competition between photoexcited carriers and piezoelectric/pyroelectric screening charges in the context of hydrogen evolution. The factor that plays a crucial role in determining the synergistic piezo-photocatalytic, pyro-photocatalytic, and piezo-pyro-photocatalytic hydrogen production should be explored. Therefore, there is an urgent need to conduct in-depth investigations into the synergistic catalytic hydrogen production mechanisms, which could offer theoretical guidance and facilitate advancements in the hydrogen production field.

Secondly, the current structure and functionality of the developed catalytic materials are relatively rudimentary, which poses significant limitations on the application of synergistic catalytic hydrogen production technology for converting natural low-density energy into chemical hydrogen energy. For example, the piezoelectric properties of most piezoelectric-photocatalytic semiconductors or piezoelectric-photocatalytic composites are generally not significant, and the piezo-photocatalytic hydrogen production typically relies on additional mechanical energy input, such as ultrasonic vibration. Furthermore, the majority of reported pyroelectric-photocatalytic materials exhibit insensitivity to environmental temperature fluctuations, necessitating additional controlled thermal variations to achieve

efficient pyro-photocatalytic hydrogen production. From the perspective of material optimization, it is imperative to enhance the piezoelectric, pyroelectric, and photocatalytic properties of catalysts through strategic composition and structural designs. The development of multifunctional catalyst composites is essential for achieving synergistic catalytic hydrogen production without reliance on additional energy input. Furthermore, the interfaces between piezoelectric/pyroelectric materials and photocatalysts must be meticulously optimized to ensure efficient coupling.

Finally, the preparation of catalysts, particularly for heterojunction catalysts and multifunctional composites, typically involves a lengthy and intricate process that is not conducive to large-scale fabrication. This severely extends the production cycle of catalysts, thereby resulting in high manufacturing costs and hindering the practical application of catalytic hydrogen production technology. From the application point of view, developing straightforward yet robust methodologies for the preparation of catalysts that exhibit high-efficiency hydrogen production, excellent stability, and cost-effectiveness is greatly desired.

DECLARATIONS

Authors' contributions

Conceptualization, writing-reviewing and editing, supervision, funding acquisition: Dai, B.

Investigation, writing-original draft, writing-reviewing and editing: Zhou, C.

Investigation, writing-reviewing and editing: Yin, H.

Visualization, writing-reviewing and editing: Kong, R.

Visualization, writing-reviewing and editing: Wang, H.

Writing-reviewing and editing, supervision, funding acquisition: Xie, Y.

Availability of data and materials

The datasets supporting the findings of this study are available from the corresponding authors upon reasonable request.

Financial support and sponsorship

This work was financially supported by the National Natural Science Foundation of China (Nos. 22202106, 61974071, and 82301104), China Postdoctoral Science Foundation (No. 2023M731772), National Key Research and Development Program of China (Nos. 2021YFA1202904, 2017YFA0205302), the Priority Academic Program Development of Jiangsu Higher Education Institutions (PAPD, No. YX030003), and the Jiangsu Provincial Key Research and Development Program (No. BE2018732).

Ethical approval and consent to participate

Not applicable.

Conflicts of interest

The authors declared that there are no conflicts of interest.

Consent for publication

Not applicable.

Copyright

© The Author(s) 2025.

REFERENCES

- Chen, Z.; Wu, H.; Li, J.; et al. Defect enhanced CoP/reduced graphene oxide electrocatalytic hydrogen production with Pt-like activity. *Appl. Catal. B. Environ.* **2020**, *265*, 118576. DOI
- Shi, Y.; Zhao, Q.; Li, J.; Gao, G.; Zhi, J. Onion-like carbon-embedded graphitic carbon nitride for enhanced photocatalytic hydrogen evolution and dye degradation. *Appl. Catal. B. Environ.* **2022**, *308*, 121216. DOI
- Bie, C.; Wang, L.; Yu, J. Challenges for photocatalytic overall water splitting. *Chem* **2022**, *8*, 1567-74. DOI
- Dingenen, F.; Verbruggen, S. W. Tapping hydrogen fuel from the ocean: a review on photocatalytic, photoelectrochemical and electrolytic splitting of seawater. *Renew. Sustain. Energy. Rev.* **2021**, *142*, 110866. DOI
- Su, H.; Pan, X.; Li, S.; Zhang, H.; Zou, R. Defect-engineered two-dimensional transition metal dichalcogenides towards electrocatalytic hydrogen evolution reaction. *Carbon. Energy.* **2023**, *5*, e296. DOI
- Du, Y.; Lu, T.; Li, X.; et al. High-efficient piezocatalytic hydrogen evolution by centrosymmetric Bi₂Fe₄O₉ nanoplates. *Nano. Energy.* **2022**, *104*, 107919. DOI
- Dai, B.; Fang, J.; Yu, Y.; et al. Construction of infrared-light-responsive photoinduced carriers driver for enhanced photocatalytic hydrogen evolution. *Adv. Mater.* **2020**, *32*, 1906361. DOI
- Zhou, P.; Navid, I. A.; Ma, Y.; et al. Solar-to-hydrogen efficiency of more than 9% in photocatalytic water splitting. *Nature* **2023**, *613*, 66-70. DOI
- Teng, J.; Li, W.; Wei, Z.; et al. Coupling photocatalytic hydrogen production with key oxidation reactions. *Angew. Chem. Int. Ed.* **2024**, *63*, e202416039. DOI
- Djellabi, R.; Ordonez, M. F.; Conte, F.; Falletta, E.; Bianchi, C. L.; Rossetti, I. A review of advances in multifunctional XTiO₃ perovskite-type oxides as piezo-photocatalysts for environmental remediation and energy production. *J. Hazard. Mater.* **2022**, *421*, 126792. DOI PubMed
- Zhang, D.; Wu, H.; Bowen, C. R.; Yang, Y. Recent advances in pyroelectric materials and applications. *Small* **2021**, *17*, 2103960. DOI
- Kim, J.; Oh, J.; Baskaran, S.; et al. Rhenium redefined as electrocatalyst: hydrogen evolution efficiency boost via Pt and Ni doping. *Appl. Catal. B. Environ. Energy.* **2024**, *347*, 123791. DOI
- Aziz, S. T.; Sultana, S.; Kumar, A.; Riyajuddin, S.; Pal, M.; Dutta, A. Transition metal phosphides as cardinal electrocatalytic materials for alkaline hydrogen production. *Cell. Rep. Phys. Sci.* **2023**, *4*, 101747. DOI
- Bai, H.; Chen, D.; Ma, Q.; et al. Atom doping engineering of transition metal phosphides for hydrogen evolution reactions. *Electrochem. Energy. Rev.* **2022**, *5*, 24. DOI
- Zhang, L.; Zhu, J.; Wang, Z.; Zhang, W. 2D MoSe₂/CoP intercalated nanosheets for efficient electrocatalytic hydrogen production. *Int. J. Hydrogen. Energy.* **2020**, *45*, 19246-56. DOI
- Saha, A.; Paul, A.; Srivastava, D. N.; Panda, A. B. Exfoliated colloidal MoS₂ nanosheet with predominantly 1T phase for electrocatalytic hydrogen production. *Int. J. Hydrogen. Energy.* **2020**, *45*, 18645-56. DOI
- Zhang, M.; Duan, Z.; Cui, L.; et al. A phosphorus modified mesoporous AuRh film as an efficient bifunctional electrocatalyst for urea-assisted energy-saving hydrogen production. *J. Mater. Chem. A.* **2022**, *10*, 3086-92. DOI
- Zhang, Z.; Liu, S.; Zhou, Y.; et al. Engineering ultrafine PtIr alloy nanoparticles into porous nanobowls via a reactive template-engaged assembly strategy for high-performance electrocatalytic hydrogen production. *J. Mater. Chem. A.* **2024**, *12*, 10148-56. DOI
- Chung, W.; Mekhemer, I. M.; Mohamed, M. G.; et al. Recent advances in metal/covalent organic frameworks based materials: their synthesis, structure design and potential applications for hydrogen production. *Coord. Chem. Rev.* **2023**, *483*, 215066. DOI
- Wang, C. P.; Lin, Y. X.; Cui, L.; Zhu, J.; Bu, X. H. 2D metal-organic frameworks as competent electrocatalysts for water splitting. *Small* **2023**, *19*, 2207342. DOI
- Zhang, L.; Wang, W.; Xu, G.; Song, H.; Yang, L.; Jia, D. Facile synthesis of Co_xFe_{1-x}P microcubes derived from metal-organic frameworks for efficient oxygen evolution reaction. *J. Colloid. Interface. Sci.* **2019**, *554*, 202-9. DOI
- Wang, Y.; Wu, J. M. Effect of controlled oxygen vacancy on H₂-production through the piezocatalysis and piezophotonics of ferroelectric R3C ZnSnO₃ nanowires. *Adv. Funct. Mater.* **2020**, *30*, 1907619. DOI
- Kuru, T.; Sarilmaz, A.; Aslan, E.; Ozel, F.; Hatay, P. I. Photo-enhanced piezocatalytic hydrogen evolution using *in situ* silver piezodeposited scheelite-type BaMoO₄ and BaWO₄. *J. Mater. Chem. A.* **2024**, *12*, 1764-71. DOI
- Wang, S.; Tian, W.; Han, J.; et al. Interfacial self-assembly-induced lattice distortion in Ti₃C₂ for enhanced piezocatalytic activity. *ACS Appl. Mater. Interfaces.* **2023**, *15*:55129-38. DOI
- Shi, W.; Guo, F.; Li, M.; Shi, Y.; Tang, Y. N-doped carbon dots/CdS hybrid photocatalyst that responds to visible/near-infrared light irradiation for enhanced photocatalytic hydrogen production. *Sep. Purif. Technol.* **2019**, *212*, 142-9. DOI
- Zhang, M.; Hu, Q.; Ma, K.; Ding, Y.; Li, C. Pyroelectric effect in CdS nanorods decorated with a molecular Co-catalyst for hydrogen evolution. *Nano. Energy.* **2020**, *73*, 104810. DOI
- Zhang, Y.; Kumar, S.; Marken, F.; et al. Pyro-electrolytic water splitting for hydrogen generation. *Nano. Energy.* **2019**, *58*, 183-91. DOI
- You, H.; Li, S.; Fan, Y.; et al. Accelerated pyro-catalytic hydrogen production enabled by plasmonic local heating of Au on pyroelectric BaTiO₃ nanoparticles. *Nat. Commun.* **2022**, *13*, 6144. DOI PubMed PMC
- Shi, W.; Chen, Z.; Lu, J.; et al. Construction of ZrC@ZnIn₂S₄ core-shell heterostructures for boosted near-infrared-light driven photothermal-assisted photocatalytic H₂ evolution. *Chem. Eng. J.* **2023**, *474*, 145690. DOI

30. Chen, M.; Li, B.; Ma, K.; et al. Efficient photocatalytic hydrogen production over copper-molybdate coupled with Meso-TiO₂ under low concentration of sacrificial agent. *Int. J. Hydrogen. Energy*. **2024**, *59*, 1042-53. DOI
31. Yang, L.; Yuan, J.; Wang, G.; et al. Construction of Tri-functional HOFs material for efficient selective adsorption and photodegradation of bisphenol a and hydrogen production. *Adv. Funct. Mater.* **2023**, *33*, 2300954. DOI
32. Wang, J.; Tian, J.; Han, P.; et al. Enhanced photocatalytic hydrogen production activity driven by TiO₂/(MoP/CdS): insights from powder particles to thin films. *Langmuir* **2024**, *40*, 21161-70. DOI
33. Huang, G.; Ye, W.; Lv, C.; et al. Hierarchical red phosphorus incorporated TiO₂ hollow sphere heterojunctions toward superior photocatalytic hydrogen production. *J. Mater. Sci. Technol.* **2022**, *108*, 18-25. DOI
34. Zheng, H.; Wang, Y.; Liu, J.; wang, J.; Yan, K.; Zhu, K. Recent advancements in the use of novel piezoelectric materials for piezocatalytic and piezo-photocatalytic applications. *Appl. Catal. B. Environ.* **2024**, *341*, 123335. DOI
35. Feng, X.; Shang, H.; Zhou, J.; et al. Heterostructured core-shell CoS_{1.097}@ZnIn₂S₄ nanosheets for enhanced photocatalytic hydrogen evolution under visible light. *Chem. Eng. J.* **2023**, *457*, 141192. DOI
36. Zhai, B.; Li, H.; Gao, G.; et al. A crystalline carbon nitride based near-infrared active photocatalyst. *Adv. Funct. Mater.* **2022**, *32*, 2207375. DOI
37. Wang, C.; Xie, Z.; Wang, Y.; Ding, Y.; Leung, M. K. H.; Ng, Y. H. Defects of metal halide perovskites in photocatalytic energy conversion: friend or foe? *Adv. Sci.* **2024**, *11*, 2402471. DOI
38. Lu, P.; Liu, K.; Liu, Y.; et al. Heterostructure with tightly-bound interface between In₂O₃ hollow fiber and ZnIn₂S₄ nanosheet toward efficient visible light driven hydrogen evolution. *Appl. Catal. B. Environ.* **2024**, *345*, 123697. DOI
39. Wenson, G.; Thakkar, H.; Tsai, H.; Stein, J.; Singh, R.; Nie, W. The degradation and recovery behavior of mixed-cation perovskite solar cells in moisture and a gas mixture environment. *J. Mater. Chem. A*. **2022**, *10*, 13519-26. DOI
40. Katsaiti, M.; Papadogiannis, E.; Dracopoulos, V.; Keramidias, A.; Lianos, P. Solar charging of a Zn-air battery. *J. Power. Sources*. **2023**, *555*, 232384. DOI
41. Zhou, L.; Yang, T.; Fang, Z.; et al. Boosting of water splitting using the chemical energy simultaneously harvested from light, kinetic energy and electrical energy using N doped 4H-SiC nanohole arrays. *Nano. Energy*. **2022**, *104*, 107876. DOI
42. Liu, B.; Wang, S.; Zhang, G.; et al. Tandem cells for unbiased photoelectrochemical water splitting. *Chem. Soc. Rev.* **2023**, *52*, 4644-71. DOI
43. Yao, T.; An, X.; Han, H.; Chen, J. Q.; Li, C. Photoelectrocatalytic materials for solar water splitting. *Adv. Energy. Mater.* **2018**, *8*, 1800210. DOI
44. Murugan, C.; Mary, A. S.; Velmurugan, R.; Subramanian, B.; Murugan, P.; Pandikumar, A. Investigating the interfacial charge transfer between electrodeposited BiVO₄ and pulsed laser-deposited Co₃O₄ p-n junction photoanode in photoelectrocatalytic water splitting. *Chem. Eng. J.* **2024**, *483*, 149104. DOI
45. Wang, G.; Tang, T.; Ye, K. H.; et al. Dual hole transport layers heterojunction and band alignment engineered Mo:BiVO₄ photoanodes for efficient water splitting. *Small* **2024**, *20*, 2403600. DOI
46. Zhang, F.; Yu, X.; Qian, Y.; et al. Multistage charge redistribution constructing heterostructured WO₃@RuSe₂ on Si for enhanced photoelectrochemical hydrogen evolution. *Chem. Eng. J.* **2022**, *446*, 137462. DOI
47. Bashiri, R.; Irfan, M. S.; Mohamed, N. M.; et al. Hierarchically SrTiO₃@TiO₂@Fe₂O₃ nanorod heterostructures for enhanced photoelectrochemical water splitting. *Int. J. Hydrogen. Energy*. **2021**, *46*, 24607-19. DOI
48. Kim, Y. K.; Lee, T. H.; Yeop, J.; et al. Hetero-tandem organic solar cells drive water electrolysis with a solar-to-hydrogen conversion efficiency up to 10%. *Appl. Catal. B. Environ.* **2022**, *309*, 121237. DOI
49. Seo, S.; Lee, J.; Kim, Y.; et al. A long-term stable organic semiconductor photocathode-based photoelectrochemical module system for hydrogen production. *J. Mater. Chem. A*. **2022**, *10*, 13247-53. DOI
50. Gong, L.; Xuan, N.; Gu, G.; et al. Power management and system optimization for high efficiency self-powered electrolytic hydrogen and formic acid production. *Nano. Energy*. **2023**, *107*, 108124. DOI
51. Ghosh, K.; Iffelsberger, C.; Konečný, M.; Vyskočil, J.; Michalička, J.; Pumera, M. Nanoarchitectonics of triboelectric nanogenerator for conversion of abundant mechanical energy to green hydrogen. *Adv. Energy. Mater.* **2023**, *13*, 2203476. DOI
52. Zhang, W.; He, W.; Dai, S.; et al. Wave energy harvesting based on multilayer beads integrated spherical TENG with switch triggered instant discharging for self-powered hydrogen generation. *Nano. Energy*. **2023**, *111*, 108432. DOI
53. Wang, X.; Yang, Q.; Singh, S.; et al. Topological semimetals with intrinsic chirality as spin-controlling electrocatalysts for the oxygen evolution reaction. *Nat. Energy*. **2025**, *10*, 101-9. DOI
54. Sun, Q.; He, J.; Nagao, A.; Ni, Y.; Wang, S. Corrigendum to “hydrogen-prompted heterogeneous development of dislocation structure in Ni” [Acta Materialia 246 (2023) 118660]. *Acta. Mater.* **2024**, *270*, 119840. DOI
55. Pei, A.; Xie, R.; Zhu, L.; et al. Methanol-enhanced low-cell-voltage hydrogen generation at industrial-grade current density by triadic active sites of Pt₁-Pd_n-(Ni₂Co)(OH)_x. *J. Am. Chem. Soc.* **2025**, *147*, 3185-94. DOI
56. Wang, S.; Song, C.; Cai, Y.; et al. Interfacial polarization triggered by covalent-bonded MXene and black phosphorus for enhanced electrochemical nitrate to ammonia Conversion. *Adv. Energy. Mater.* **2023**, *13*, 2301136. DOI
57. Thakur, D.; Porwal, C.; Singh, C. V.; Balakrishnan, V.; Vaish, R. 2D transition metal dichalcogenides: synthesis methods and their pivotal role in photo, piezo, and photo-piezocatalytic processes. *Sep. Purif. Technol.* **2024**, *337*, 126462. DOI
58. Han, Q.; Han, Z.; Wang, Y.; et al. Enhanced photocatalytic hydrogen evolution by piezoelectric effects based on MoSe₂/Se-decorated CdS nanowire edge-on heterostructure. *J. Colloid. Interface. Sci.* **2023**, *630*, 460-72. DOI

59. Wang, W.; Zhang, M.; Li, X.; et al. Boosting efficiency in piezo-photocatalysis process using poled Ba_{0.7}Sr_{0.3}TiO₃ nanorod arrays for pollutant degradation and hydrogen production. *ACS. Appl. Mater. Interfaces*. **2024**, *16*, 20497-509. DOI
60. Tu, S.; Wang, Y.; Huang, H.; et al. Enhanced charge carrier separation by bi-piezoelectric effects based on pine needle-like BaTiO₃/ZnO continuous nanofibers. *J. Mater. Chem. A*. **2022**, *10*, 13544-55. DOI
61. Jin, X.; Li, X.; Dong, L.; et al. Enhancement and inhibition of photocatalytic hydrogen production by fine piezoelectric potential tuning over piezo-photocatalyst. *Nano. Energy*. **2024**, *123*, 109341. DOI
62. Yang, Z.; Xia, X.; Fang, M.; wang, L.; Pan, S.; guo, Y. Promoting the electron/hole co-extraction using piezotronic effect in Pt/ZnIn₂S₄/BaTiO₃ heterojunctions for photocatalytic synergistic hydrogen evolution and HMF oxidation. *Mater. Today. Phys.* **2023**, *36*, 101158. DOI
63. Guo, M.; Zhong, J.; Li, W.; et al. Highly-efficient photocatalytic hydrogen evolution enabled by piezotronic effects in SrTiO₃/BaTiO₃ nanofiber heterojunctions. *Nano. Energy*. **2024**, *127*, 109745. DOI
64. Wei, H.; Zhou, L.; Cao, F.; et al. Constructing magnetically propelled piezoelectric and pyroelectric bifunctional micromotors to boost the photocatalytic H₂ production involving biomass reforming. *Nano. Energy*. **2024**, *129*, 110064. DOI
65. Zhang, S.; Chen, D.; Liu, Z.; Ruan, M.; Guo, Z. Novel strategy for efficient water splitting through pyro-electric and pyro-photo-electric catalysis of BaTiO₃ by using thermal resource and solar energy. *Appl. Catal. B. Environ.* **2021**, *284*, 119686. DOI
66. Zhang, S.; Zhang, B.; Chen, D.; Guo, Z.; Ruan, M.; Liu, Z. Promising pyro-photo-electric catalysis in NaNbO₃ via integrating solar and cold-hot alternation energy in pyroelectric-assisted photoelectrochemical system. *Nano. Energy*. **2021**, *79*, 105485. DOI